

CHAPTER 5

Results and Discussion

In this section, we will present and discuss the results of our calculations on electron/positron-Rb scattering. Where possible, we will compare the results with the available theoretical and experimental data. The elastic, excitation, total and differential cross sections will be presented.

5.1 List of Calculations

The atomic wavefunction used in the present calculations is represented by a single configuration Hartree-Fock representation, with the one-electron bound state expressed in terms of a Slater expansion. The wavefunctions are obtained from Y. J. Zhou (personal communication, January 15, 2009). Following Zhang *et al.* (2007), the wavefunctions are calculated using the SCHF (Single-configuration Hartree-Fock). The CCO calculations for electron-Rb scattering were done using the computational codes developed by McCarthy and Stelbovics (1983a). The CC(m,n) and CCO(m,n) calculations for positron-Rb scattering were done using the codes developed by Mitroy (1993a).

The following calculations were implemented in this thesis:

5.1.1 Electron-Rb Scattering

- (i) CC5 : Close-coupling (CC) method which includes the first 5 Rb atomic states (5s, 5p, 4d, 6s, 6p).
- (ii) CCO5 : The first 5 Rb atomic states are used together with the continuum optical potentials for the 5s-5s, 5s-5p and 5p-5p coupling.

(iii) CC8 : Close-coupling (CC) method which includes the first 8 Rb atomic states (5s, 5p, 4d, 6s, 6p, 5d, 7s, 7p).

(iv) CCO8 : The 8 Rb atomic states in (iii) are used together with the continuum optical potentials for the 5s-5s, 5s-5p and 5p-5p coupling.

(v) UBA8 : Unitarized Born approximation including the first 8 Rb atomic states (5s, 5p, 4d, 6s, 6p, 5d, 7s, 7p).

5.1.2 Positron-Rb Scattering

(i) CC(5,3) : Close-coupling (CC) method that includes the first 5 Rb atomic states (5s, 5p, 4d, 6s, 6p) together with 3 positronium states (1s, 2s, 2p).

(ii) CC(5,6) : Close-coupling (CC) method that includes the first 5 Rb atomic states (5s, 5p, 4d, 6s, 6p) together with 6 positronium states (1s, 2s, 2p, 3s, 3p, 3d).

(iii) CC(8,3) : Close-coupling (CC) method that includes the first 8 Rb atomic states (5s, 5p, 4d, 6s, 6p, 5d, 7s, 7p) together with 3 positronium states (1s, 2s, 2p).

(iv) CC(8,6) : Close-coupling (CC) method that includes the first 8 Rb atomic states (5s, 5p, 4d, 6s, 6p, 5d, 7s, 7p) together with 6 positronium states (1s, 2s, 2p, 3s, 3p, 3d).

(v) CCO(5,3) : The 8 states in (i) are used together with the continuum optical potentials in the 5s-5s, 5s-5p and 5p-5p coupling.

(vi) CCO(5,6) : The 11 states in (ii) are used together with the continuum optical potentials in the 5s-5s, 5s-5p and 5p-5p coupling.

(vii) CCO(8,3) : The 11 states in (iii) are used together with the continuum optical potentials in the 5s-5s, 5s-5p and 5p-5p coupling.

(viii) CCO(8,6) : The 14 states in (iv) are used together with the continuum optical potentials in the 5s-5s, 5s-5p and 5p-5p coupling.

5.2 Electron-Rubidium Scattering

5.2.1 Elastic and Inelastic Cross Sections

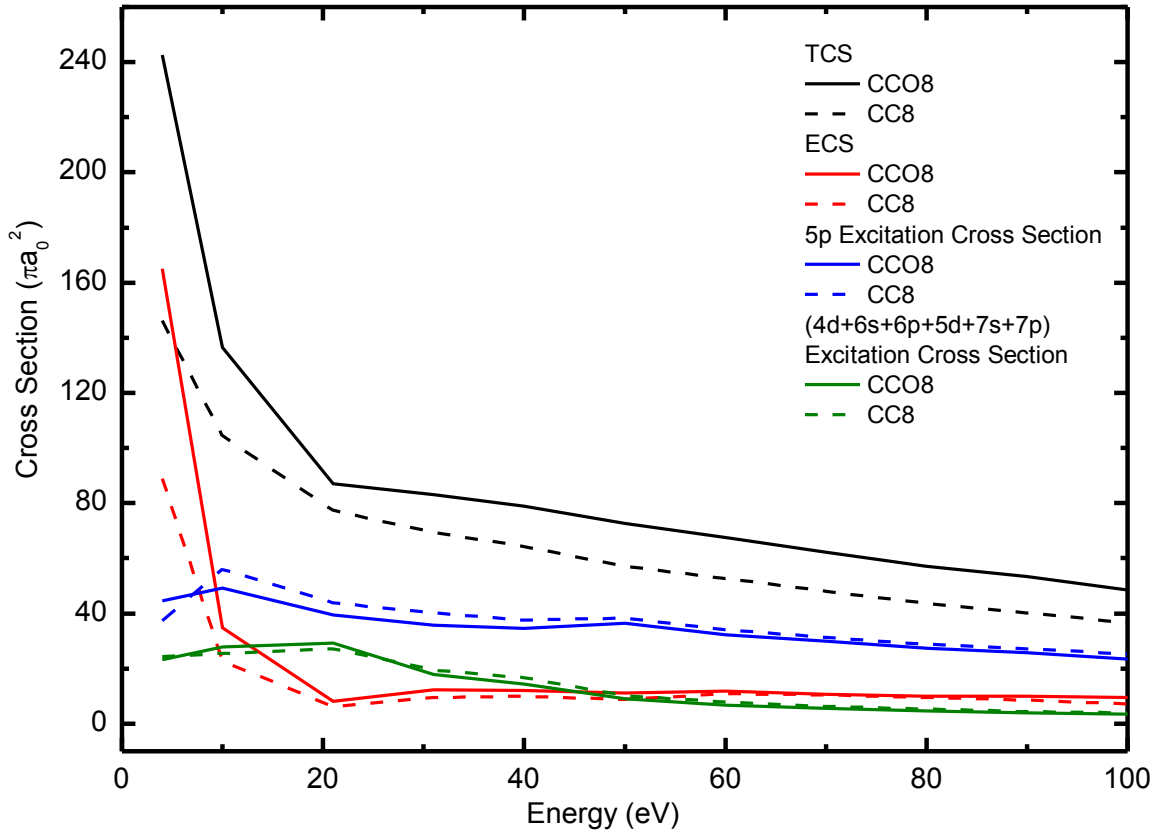


Fig. 5.1 : The total, elastic and inelastic cross sections of the electron-Rb scattering.

Figure 5.1 shows the elastic (ECS), inelastic and total cross sections of electron-Rb scattering. We can observe that the overall TCS is generally dominated by the 5p inelastic channel but below 10 eV, the elastic channel dominates. This is expected due to the large dipole polarization of Rb. We observe that the contribution from the larger discrete states are also significant. In general, the continuum effect increases the CCO8 ECS. The contributions of each channel to the TCS for CC8 and CCO8 calculations are tabulated in Table 5.1 and Table 5.2. In Table 5.1, we can observe that the 5p channel contributes 50% - 70% to the TCS, thus making it the primary dominant channel. The

5s channel is the secondary dominant channel which contributes 10% - 20% to the TCS except at 20 eV. At 4 eV, the 5s channel is much more important than the 5p channel by contributing more than 60% to the TCS. The other channels (4d, 6s, 6p, 5d, 7s, 7p) are less important in the scattering process as they contribute relatively lesser to the TCS (<10%). The continuum effect in CCO8 model has increased the contribution of 5s channel from 10% - 20% to 10% - 30%. The 5p channel remains as the primary channel which contributes 50% - 65% to the TCS, except at 10 eV. The other channels are still less significant compared to the 5s and 5p channels.

Table 5.1 : The cross sections for different channels at various energies for the CC8 calculations of electron-Rb scattering.

Energy (eV)	Cross Section (πa_0^2)							
	5s	5p	4d	6s	6p	5d	7s	7p
4	88.88	37.45	4.48	2.68	3.52	6.02	4.98	2.61
10	22.82	56.16	10.09	2.50	5.85	1.38	1.13	4.48
21	6.26	43.96	8.00	5.84	6.35	2.02	3.70	1.26
31	9.48	40.26	0.77	0.78	5.38	4.58	4.59	3.46
40	10.00	37.49	1.82	0.62	1.89	7.06	4.14	1.20
50	8.74	38.20	1.79	0.44	1.52	4.76	1.39	0.36
60	10.86	34.07	1.49	0.67	0.92	3.16	1.25	0.33
70	10.53	31.23	1.25	0.71	0.85	2.30	0.95	0.27
80	9.61	28.89	1.12	0.61	0.73	1.85	0.72	0.22
90	8.51	27.11	0.92	0.52	0.65	1.57	0.60	0.19
100	7.25	25.35	0.75	0.39	0.59	1.55	0.49	0.16

Table 5.2 : The cross sections for different channels at various energies for the CCO8 calculations of electron-Rb scattering.

Energy (eV)	Cross Section (πa_0^2)							
	5s	5p	4d	6s	6p	5d	7s	7p

4	165.02	44.64	6.30	4.03	5.10	1.07	1.07	5.66
10	34.88	49.20	9.44	5.44	6.65	1.30	1.01	4.02
21	8.00	39.44	7.26	7.61	7.22	1.71	4.21	1.29
31	12.22	35.80	0.72	0.65	5.41	4.15	3.95	3.02
40	12.00	34.51	1.63	0.24	2.07	5.93	3.63	0.88
50	11.18	36.38	1.59	0.43	1.53	3.94	1.23	0.29
60	11.86	32.14	1.38	0.61	0.89	2.64	1.02	0.29
70	10.58	29.87	1.16	0.61	0.80	1.96	0.80	0.25
80	10.01	27.27	1.03	0.54	0.69	1.57	0.60	0.21
90	10.08	25.65	0.85	0.47	0.64	1.34	0.47	0.18
100	9.49	23.45	0.67	0.33	0.60	1.31	0.35	0.16

5.2.2 Total Cross Section (TCS)

In Figure 5.2 the TCS for electron-rubidium scattering are depicted. The present calculations are compared with the modified Glauber approximation (MG3) (Gien (1993)) and the available experimental data (Parikh *et al.* (1993), Stein *et al.* (1990)). In general, the CC8 model is in good agreement with the experimental data over the scattering energies studied. Although the CCO8 calculation displays similar qualitative features as the experimental measurements, it overestimates the TCS. At energies lower than 20 eV, the CCO8 model increases drastically but it is still within the experimental data error bars. In contrast, the UBA8 calculation agrees reasonably well with the experimental data at energies higher than 50 eV. We note that the CC8, UBA8 and MG3 calculations converge at higher energies. The CCO8 TCS is overall higher in magnitude than the other models due to the continuum effect. The continuum effect continues to remain significant at all energies except at 20 eV.

Following the recent research on the forward angle scattering effects by Sullivan *et al.* (2011), the discrimination against the forward scattering will cause significant changes in the TCS. Furthermore, the large dipole polarizability of Rb will have significant effect on the magnitude of the forward scattering. Sullivan *et al.* (2011) demonstrates that the increasing neglect of the forward scattering will cause the

magnitude of the TCS to decrease. We note that in the Parikh *et al.* (1993) experiment, their measurement uncertainty estimation does not allow the angular-discrimination consideration. Since Parikh *et al.* (1993) ignore the discrimination, so their measured TCS are supposed to be lower than the ‘real’ TCS. Thus, it is plausible that the present CCO8 calculation is a reliable approach as its cross sections are generally higher than the measured TCS by Parikh *et al.* (1993).

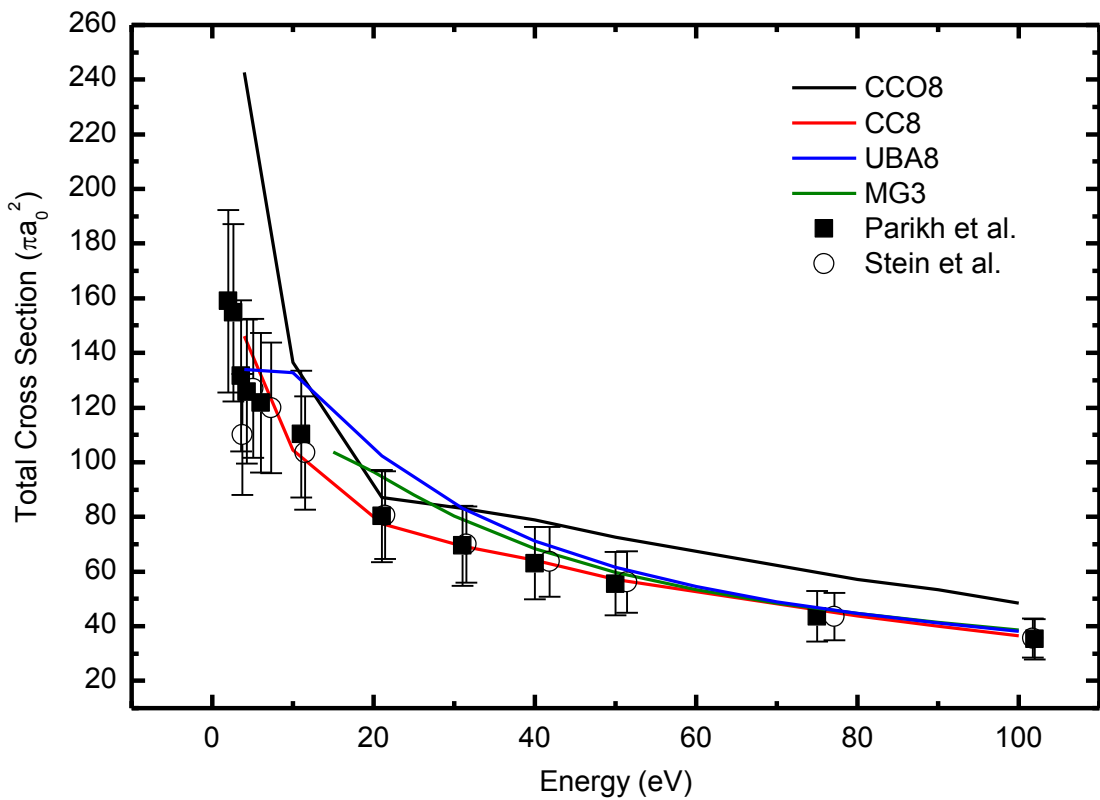


Fig. 5.2 : TCS of electron-Rb scattering for energy ranged from 10 eV to 100 eV.

5.2.3 Differential Cross Section (DCS)

a) Elastic Transition

i) 10 eV

Figure 5.3 shows the DCS of electron-Rb elastic scattering at 10 eV. Our calculations do not agree well with the experiment data quantitatively and qualitatively. Generally, the CC8 and CCO8 models' underestimates the DCS and predict some qualitative features which are not seen in the experiment data. However, it is gratifying to note that both models display similar qualitative trends where there is a shoulder at the forward scattering region and 2 minima at the middle and backward angles. The minimum of CC8 calculation at the backward angle is a deeper than the one predicted by the CCO8 calculation. The continuum effect is seen to be insignificant at 10 eV as the CCO8 DCS does not differ much in magnitude compared to the CC8 DCS while showing qualitative similarities. In general, the UBA8 calculation is also in accord with the CCO8/CC8 models but it only predicts one minimum at the middle angle range.

ii) 20 eV

At 20 eV (Figure 5.4), both the CCO8 and CC8 models agree very well with the experimental data. In contrast to 10 eV, the continuum effect is important at 20 eV, where the DCS of the CCO8 calculation is significantly lower than the CC8 calculation over the entire scattering region. Both CCO8 and CC8 models exhibit identical qualitative trends with 3 minima at about 30° , 90° and 145° . However, the experimental data only shows a minimum at 80° . Furthermore, the experimental data also does not depict any minimum at the forward scattering region. The UBA8 calculation is in excellent agreement with the experimental data at the forward angles. However, at scattering angles larger than 50° , this model slightly underestimates the DCS while showing a minimum at the middle angle.

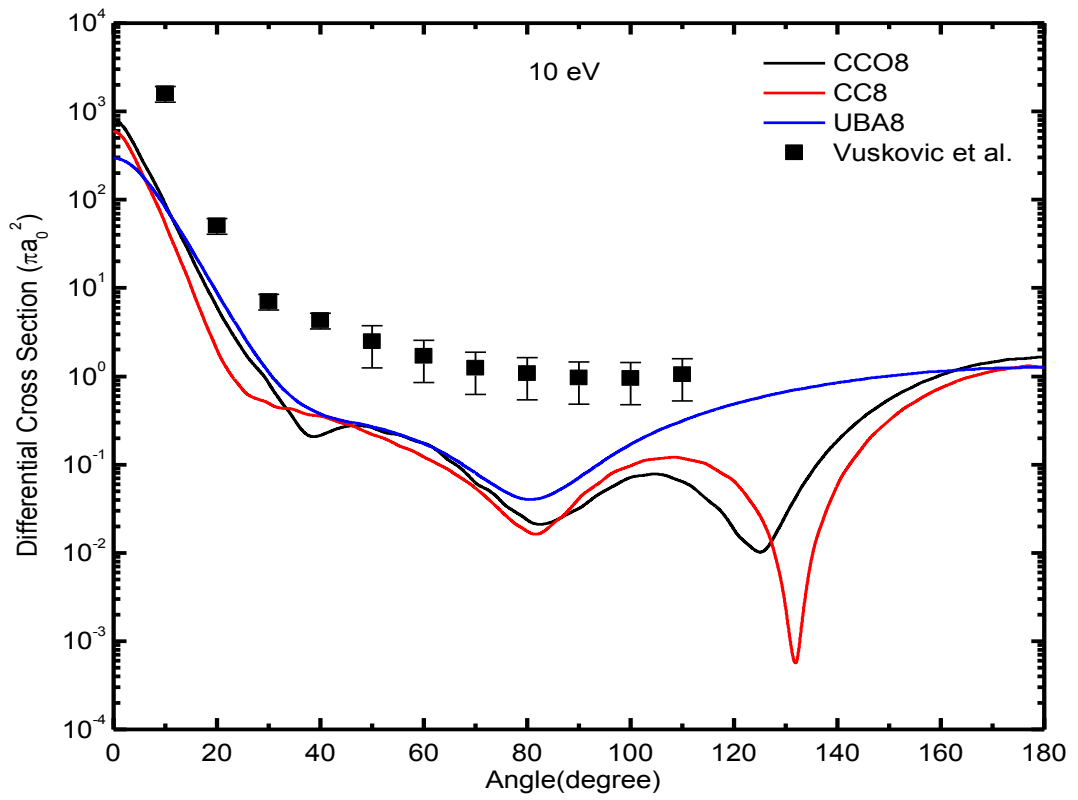


Fig. 5.3 : DCS of electron-Rb elastic scattering at 10 eV.

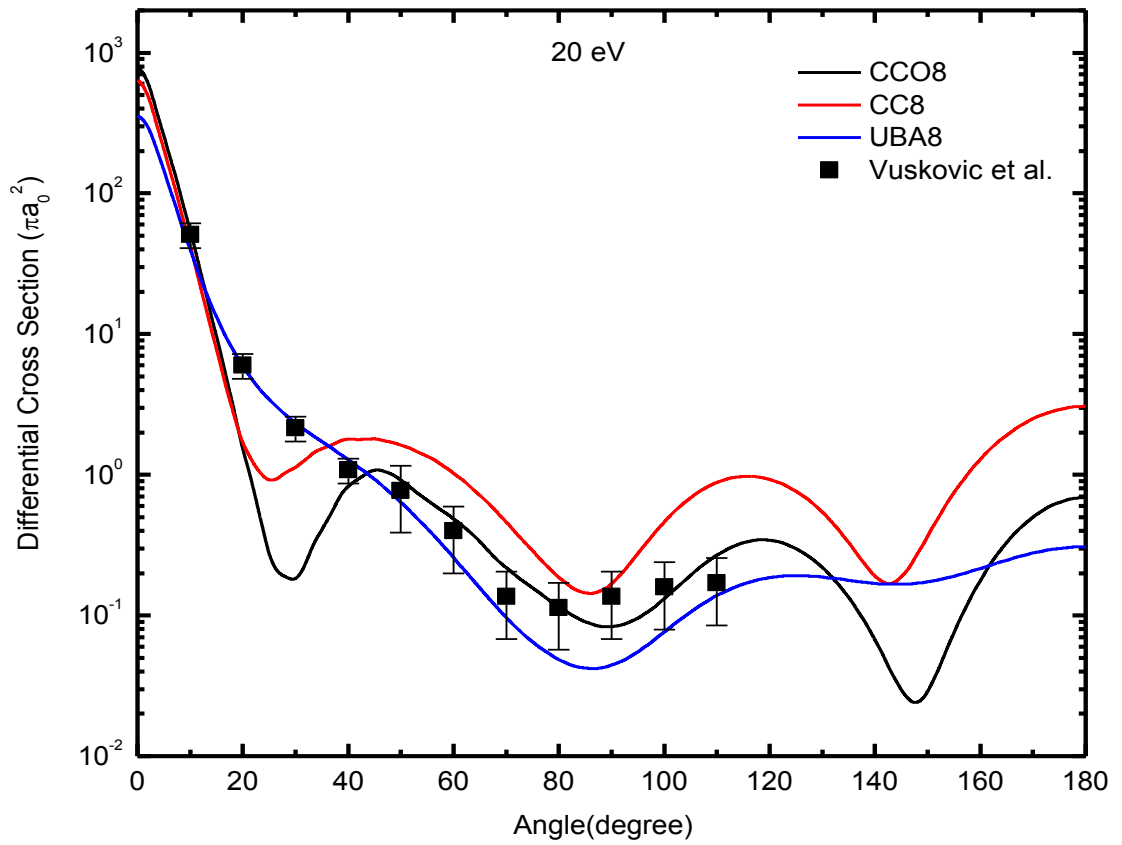


Fig. 5.4 : DCS of electron-Rb elastic scattering at 20 eV.

iii) 30-100 eV

In this energy range, the lack of experimental and theoretical data limits our discussion. However, for completeness, we present some of the main features of our calculations in Figures 5.5 and 5.6.

In general, the CCO8 and CC8 DCS show good consistency by having the similar qualitative shapes over the whole energy region. Both CCO8 and CC8 models display a shoulder at the forward angles, followed by a minimum at the backward angles. The shoulder shifts to the lower angles and gradually vanishes as the energy increases. For instance, we can barely observe the existence of the shoulder at 20° at 60 eV. Likewise, the minimum at the backward scattering region shifts to the lower scattering angles (from $\sim 130^\circ$ at 30 eV to $\sim 100^\circ$ at 100 eV) with increasing energy. From 40 eV onwards, a second minimum emerges at the forward scattering region. Similarly, a third minimum emerges at the backward angles from 70 eV onwards. The depth of the minima increases as the energy increases. The minor fluctuation in the DCS at 40 eV is due to the insufficient partial waves used in the calculation. The CCO8 model which includes the continuum effect is, overall, lower in magnitude than the CC8 model except at the forward angles (0° to $\sim 15^\circ$).

There are some discrepancies between the UBA8 calculation and the CCO8 and CC8 calculations. Qualitatively, UBA8 calculation does not display any minimum in the DCS. Quantitatively, the UBA8 DCS is higher than the CCO8 and CC8 DCS but lower than both of them at the middle angles.

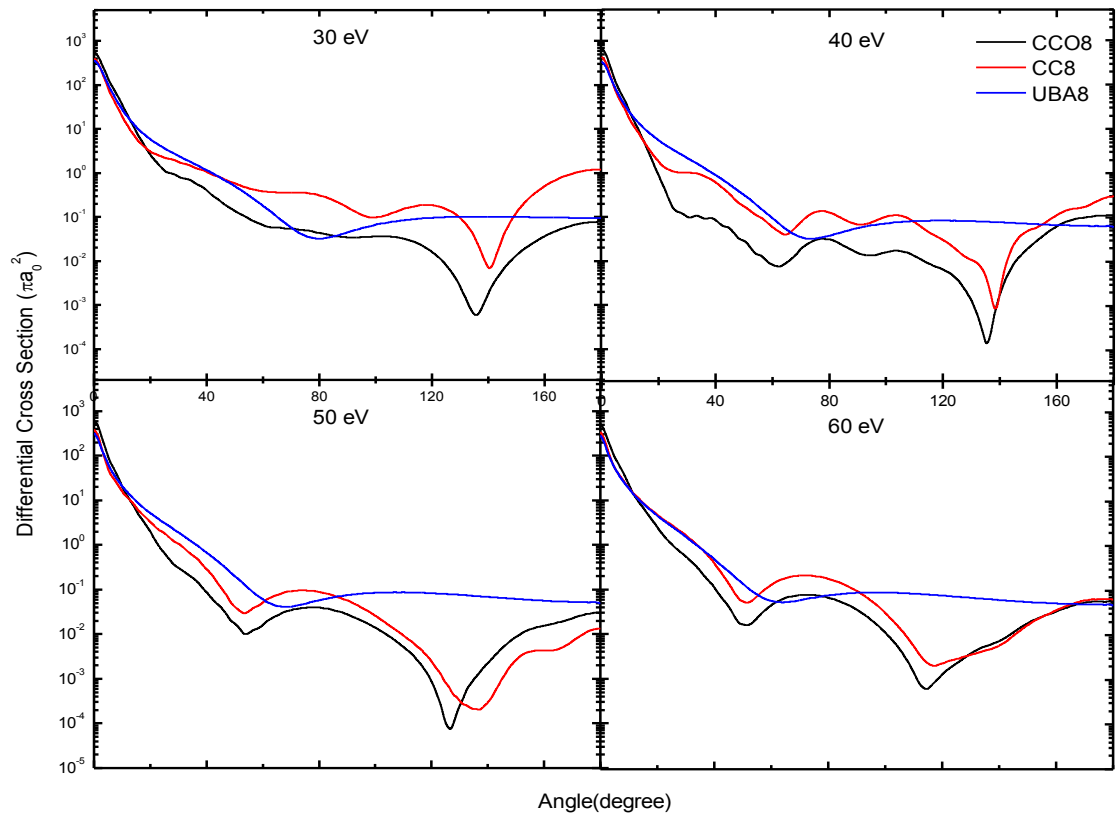


Fig. 5.5 : DCS of electron-Rb elastic scattering from 30 eV to 60 eV.

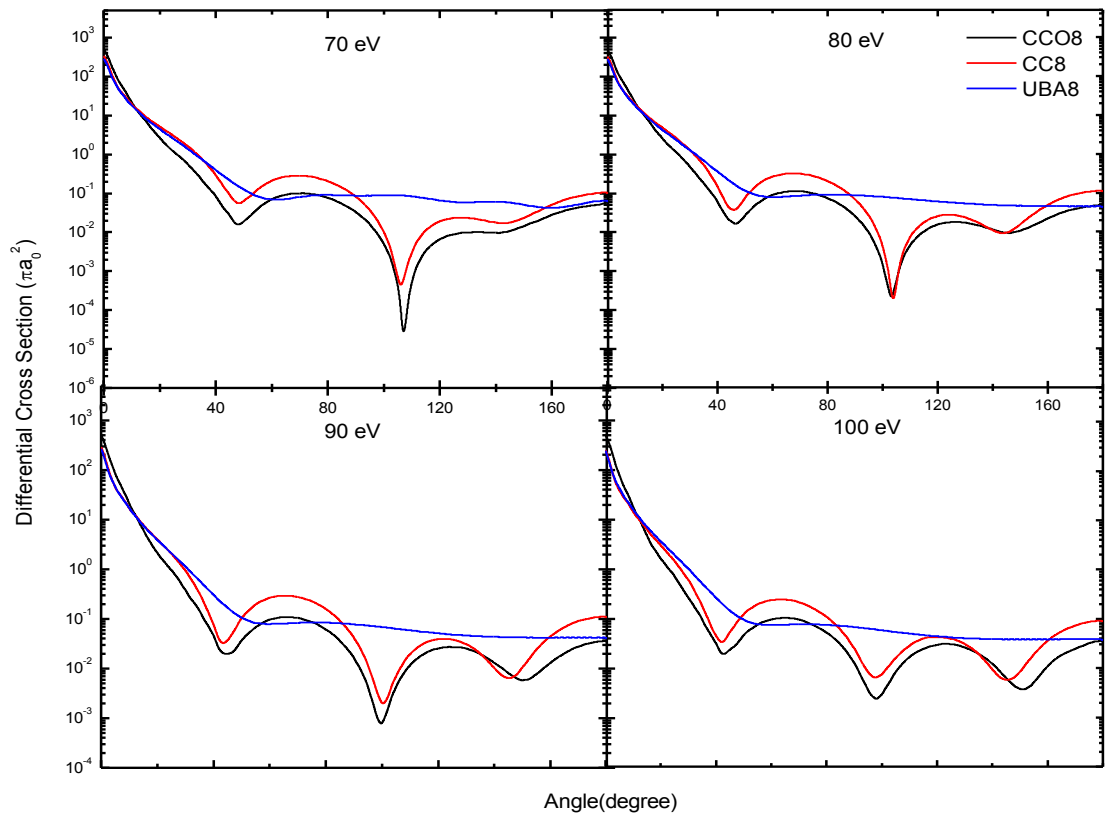


Fig. 5.6 : DCS of electron-Rb elastic scattering from 70 eV to 100 eV.

b) 5p Excitation Transition

i) 10 eV

The DCS for 5p excitation is depicted in Figure 5.7. The DWM is the distorted wave method done by Pangantiwar and Srivastava (1988). Generally, our calculations are in good accord with the experimental data. Quantitatively, the CCO8 and CC8 calculations agree extremely well with the experimental data. Our results are closer to the experimental data compared to the DWM calculation which overestimates the DCS at all the scattering angles.

Qualitatively, both of the CCO8 and CC8 models successfully predict the overall DCS shape of the experimental data but there are some discrepancies at the middle scattering region (70° - 110°). At that scattering region, they are unable to predict a minimum which is displayed by the experimental data. The CCO8 calculation predicts a shoulder at the forward angles ($\sim 20^{\circ}$) but the shoulder does not exist in the other data. At the backward scattering angles, the UBA8 calculation exhibits very different feature compared to the others. The UBA8 DCS decreases exponentially as the scattering angle increases, whereas the other models do not display this trend. Since the experimental data only show the DCS up to 110° , so we are not able to verify the qualitative features at the angles larger than 110° .

ii) 20 eV

At 20 eV (Figure 5.8), the CCO8 and CC8 calculations are in good agreement with the experiment until $\sim 50^{\circ}$. At the middle scattering region (50° to 110°), there is a discrepancy between the CCO8 and CC8 calculations and the other data. These models show a maximum in this scattering region. However, the maximum is not seen in the experimental data as well as the DWM and UBA8 calculations. Furthermore, CCO8/CC8 DCS are generally higher than the other results in this scattering region. At

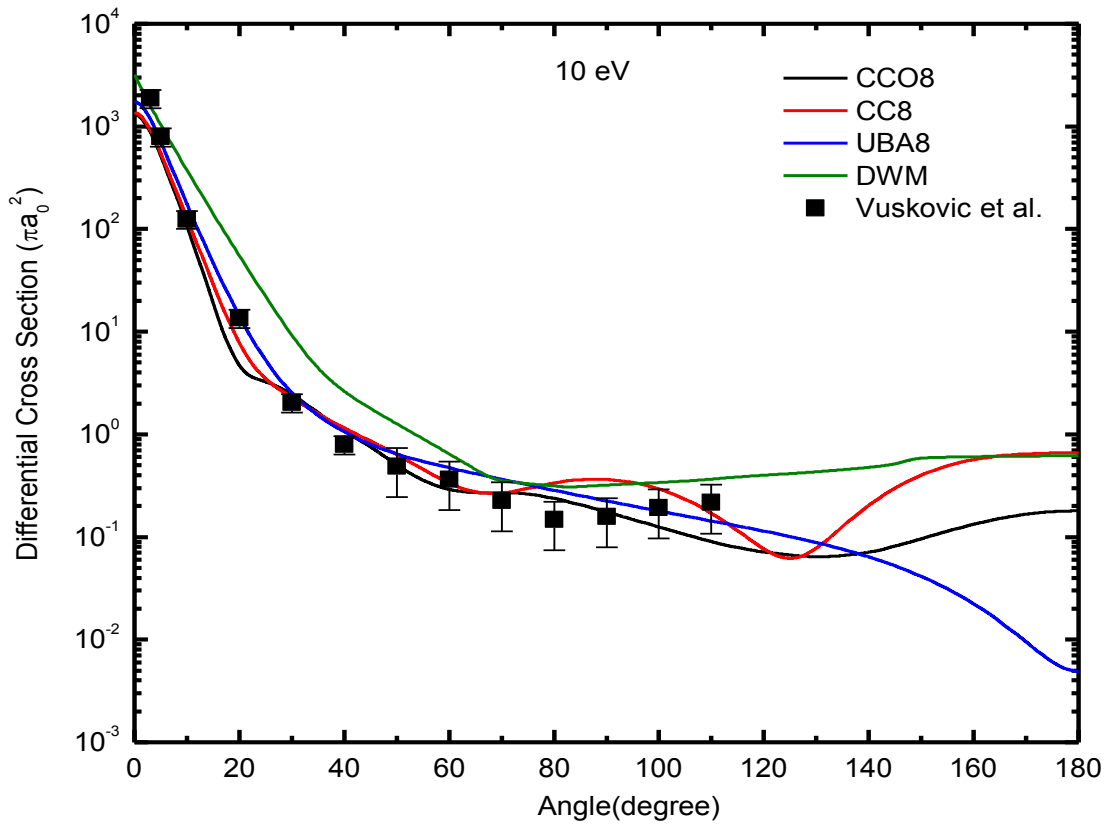


Fig. 5.7 : DCS of electron-Rb 5s-5p excitation at 10 eV.

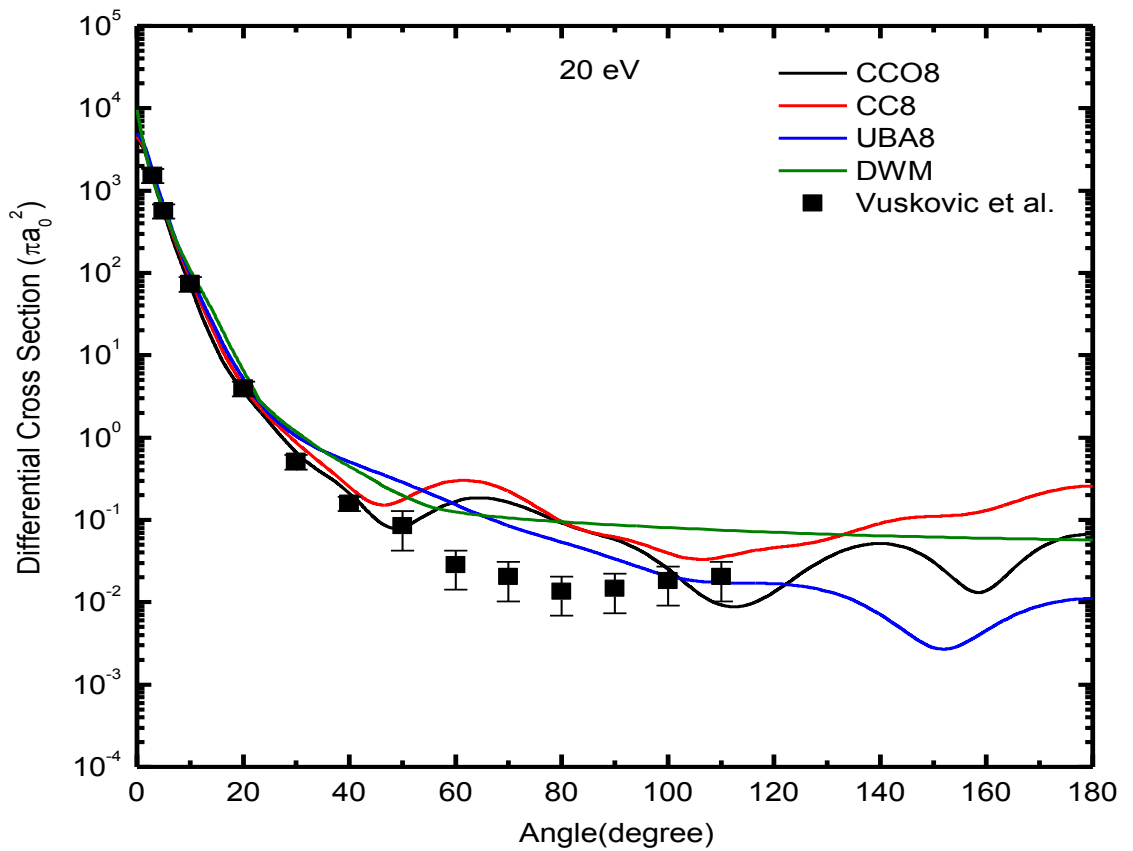


Fig. 5.8 : DCS of electron-Rb 5s-5p excitation at 20 eV.

the backward scattering region ($>110^\circ$), all the calculations show different qualitative features. It is hard to make a conclusion on the features at the backward angles as long as there is no experimental data to compare at that scattering region.

iii) 30-100 eV

The DCS of electron-Rb 5s – 5p excitation is depicted in Figures 5.9 and 5.10. Similar to the elastic scattering case, we do not have any available experimental or theoretical data to compare with our results at these energies (See Figure 5.9 and 5.10). The qualitative shapes of the DCS of the CCO8 and CC8 calculations in the 5s-5p excitation are quite similar to the qualitative shapes of the elastic scattering case. We can observe a shoulder at the forward angles and it remains in the 10° - 20° scattering region at all incident energies. There are 2 minima at $\sim 60^\circ$ and $\sim 120^\circ$ which shift to the lower scattering angles ($\sim 50^\circ$ and $\sim 110^\circ$) as the energy increases. A third minimum emerges at the backward angles at 50 eV and it gets deeper as the energy increases. The UBA8 calculation does not show any minimum or maximum over the scattering angles at all energies. At 40 eV, the CCO8 and CC8 models' DCS fluctuate, thus showing a few minima which cannot be found in the other incident energies. The fluctuation is caused by the insufficient partial waves used in the calculation. Quantitatively, the CCO8 calculation has overall lower DCS than the CC8 calculation due to the continuum effect included in the CCO8 model. The UBA8 DCS is lower than both CCO8 and CC8 calculation at angles larger than 60° .

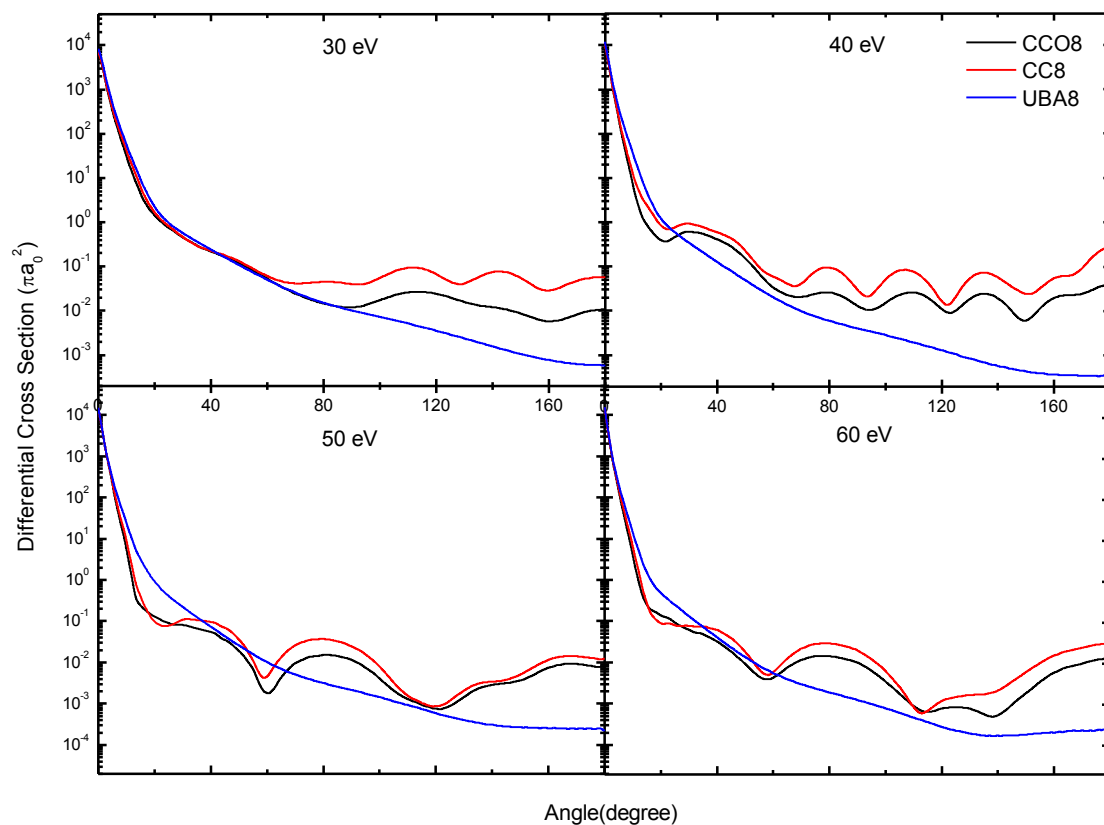


Fig. 5.9 : DCS of electron-Rb 5s-5p excitation at 30 eV to 60 eV.

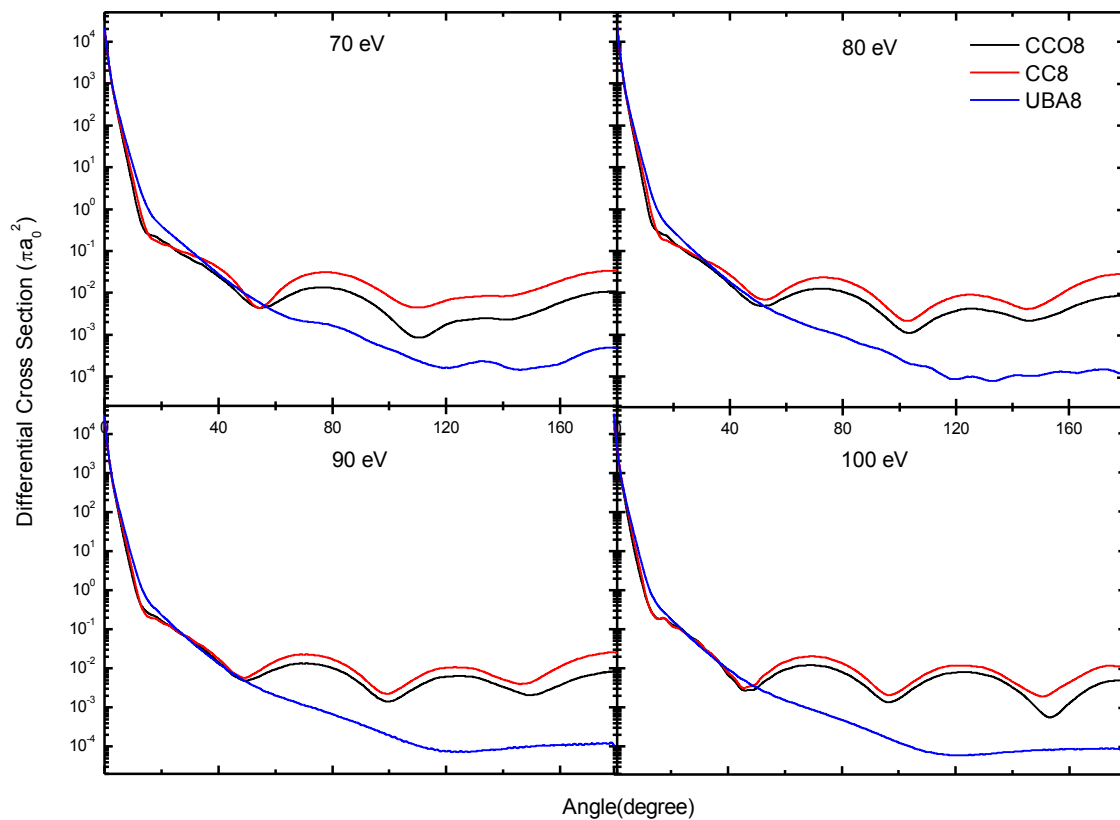


Fig. 5.10 : DCS of electron-Rb 5s-5p excitation at 70 eV to 100 eV.

5.3 Positron-Rubidium Scattering

5.3.1 Elastic and Excitation Cross Sections

In this section, the present calculated elastic and excitation cross sections with available experimental and theoretical data are compared. The discussion is limited to the 5s elastic transition and 5p, 4d, 6s, 6p excitation transitions. The cross sections are depicted in Fig 5.11 – 5.15. Although various calculations have been done as listed in Section 5.1.2, only the CCO(8,6), CCO(5,6), CC(8,6) and CC(5,6) calculations are depicted in the graphs to avoid over-cluttering. The tabulated cross sections data for all the CCO(m,n) and CC(m,n) calculations can be found in Appendix VI. The channel contributions can be found in Appendix VII.

a) Elastic Transition

Figure 5.11 shows the ECS for positron-Rb scattering. The $CC(5,6)^K$ is the 5-states R-matrix method with 6 Ps states (Kernoghan *et al.* (1996)), the $CC5^E$ and PO are the 5-states CC and the polarized-orbital calculations (McEachran *et al.* (1991)). The RCC is the 3-states relativistic CC method (Feng *et al.* (1998)). The PFMP is the parameter-free model potential calculation (Reid and Wadehra (1998)).

Generally, the present calculations are in good agreement with the other theoretical data except the PFMP calculation which overestimates the ECS at all energies. At 4 eV to 8 eV, the present calculations are in between the ECS of the $CC(5,6)^K$ and the RCC models. Our results agree very well with McEachran's results ($CC5^E$ & PO) at this energy region. We note that the ECS of our models converge with all the other data except PFMP as the energy increases. The CCO(m,n) calculations are consistent with the CC(m,n) calculations. The magnitude of the difference is not very large, indicating that the continuum effect in this transition is not significant. The

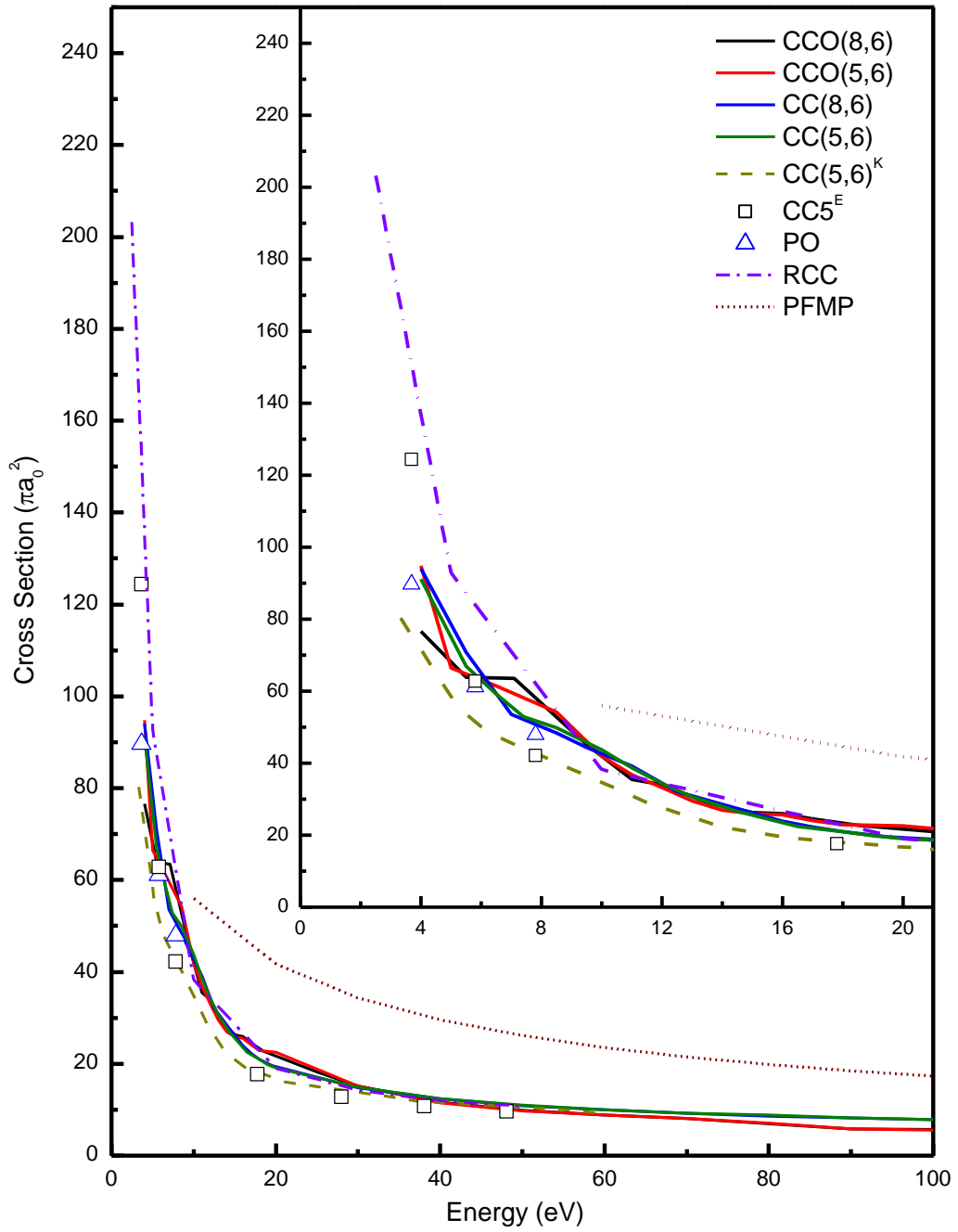


Fig. 5.11 : Elastic cross sections of positron-Rb scattering.

inclusion of the continuum channels has caused the incident flux to be absorbed into these channels instead of being scattered into the 5s channel. The loss of flux has lowered the ECS of the CCO(m,n) calculations at 40 eV to 100 eV.

From Table G.1 and G.2 in Appendix VII, it can be noted that the 5s transition is the dominant channel at 5 eV which its cross section contributes more than 35% to the TCS in both the CC(8,6) and CCO(8,6) calculations. But, its contribution decreases as the energy increases. Thus, it becomes less dominant than the 5p transition at energies larger than 10 eV.

b) 5p Excitation Transition

The cross sections of the 5p excitation are depicted in Figure 5.12. The CCO(m,n) and CC(m,n) calculations agree qualitatively well with the $CC(5,6)^K$ calculation where the models display a peak at around 15 eV and a shoulder at around 8 eV. Neither the $CC5^E$ nor the RCC models show this peak in the cross section. It can be noted that there is a minimum in the CCO(m,n) cross sections at around 16 eV, which does not exist in any of the other data. This feature may be caused by the continuum effect but we do not exclude the possibility of it being an artifact.

Quantitatively, the CCO(m,n) cross sections are overall lower than the CC(m,n) cross sections. The discrepancy is about 10% - 30%. The large difference between the CCO(m,n) and CC(m,n) models shows that the continuum effect is strong in this transition. The discrepancies decrease as the energy increases and the calculations converge gradually at high energies. The present calculations differ in magnitude with the $CC(5,6)^K$ calculation. The CCO(m,n) cross sections are lower than the $CC(5,6)^K$ calculation by 18%. In contrast, the CC(m,n) cross sections are higher than the $CC(5,6)^K$ cross section by 14%. But, the difference between the CCO(m,n) cross sections and the $CC(5,6)^K$ cross section decreases as the energy increases.

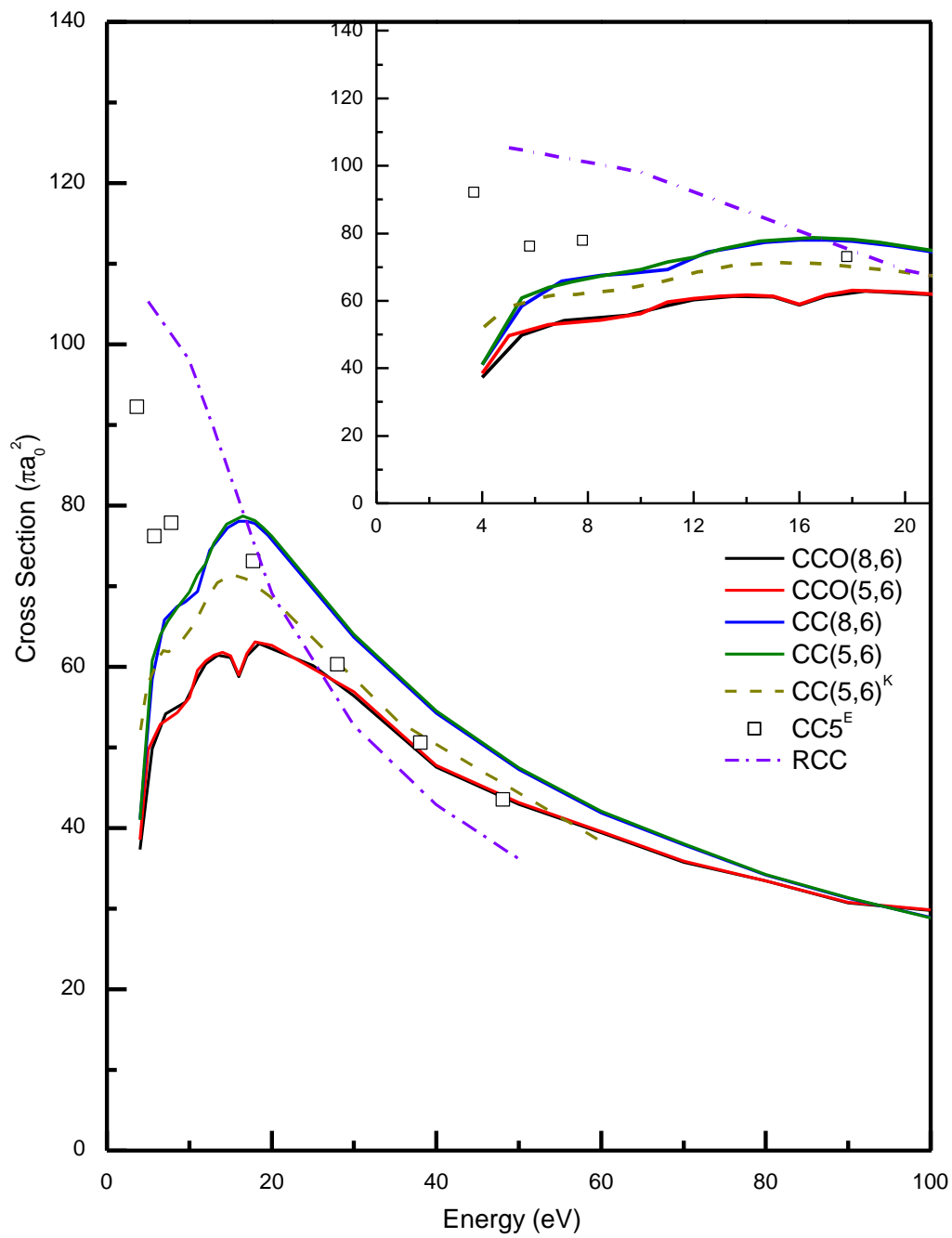


Fig. 5.12 : 5s - 5p excitation cross sections of positron-Rb scattering.

It can be observed from Table G.1 and G.2 that the contribution of the 5p transition to the TCS gradually increases as the energy increases. At 10 eV, this transition substitutes the 5s transition as the dominant channel.

c) 4d Excitation Transition

The cross sections for the 5s – 4d excitation are depicted in Figure 5.13. The present calculations agree qualitatively with the $CC(5,6)^K$ and $CC5^E$ calculations. Both the $CCO(m,n)$ and $CC(m,n)$ models are able to display a ‘peak’ at around 7 eV. Quantitatively, the $CCO(m,n)$ calculations has a lower cross sections than the $CC(m,n)$ calculations by an average of 13%. Generally, the $CCO(m,n)$ and $CC(m,n)$ models are in good agreement with the $CC(5,6)^K$ calculation. The former calculations’ cross sections are closer to the $CC(5,6)^K$ cross section at energies higher than 12 eV. On the other hand, at the energies around the ‘peak’, the $CC(m,n)$ models have better agreement with the $CC(5,6)^K$ calculation compared to the $CCO(m,n)$ models. We can observe that the $CC5^E$ calculation overestimates the cross section at energies lower than 20 eV. The cross section of $CC5^E$ calculation at about 4 eV, 6 eV and 8 eV are almost 3 times higher than the other calculations. The overestimation is probably caused by the omission of the Ps states. As the incident energy increases, all the calculations eventually converge. The contribution of the 4d transition to the TCS is relatively lesser compared to the 5s and 5p transition (refer to Table G.1 and G.2). In general, this transition contributes less than 11% and 16% to the TCS in the $CC(8,6)$ and $CCO(8,6)$ calculations.

d) 6s Excitation Transition

Figure 5.14 shows the cross sections of 5s – 6s excitation transition. In general, the $CC(m,n)$ and $CCO(m,n)$ calculations agree fairly well with the $CC(5,6)^K$ calculations. Both of the calculations predict a minimum at the energy region from 12

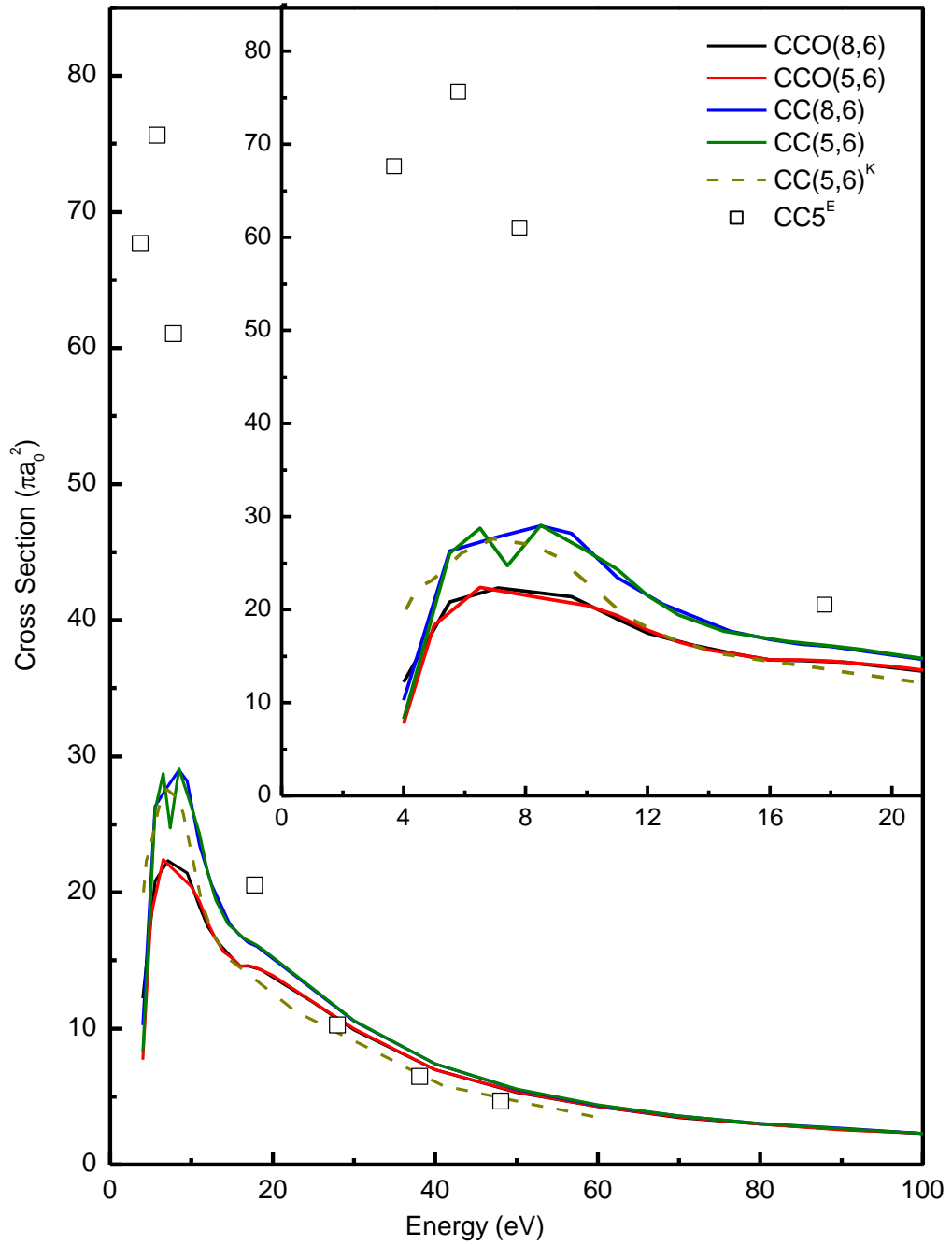


Fig. 5.13 : 5s – 4d excitation cross sections of positron-Rb scattering.

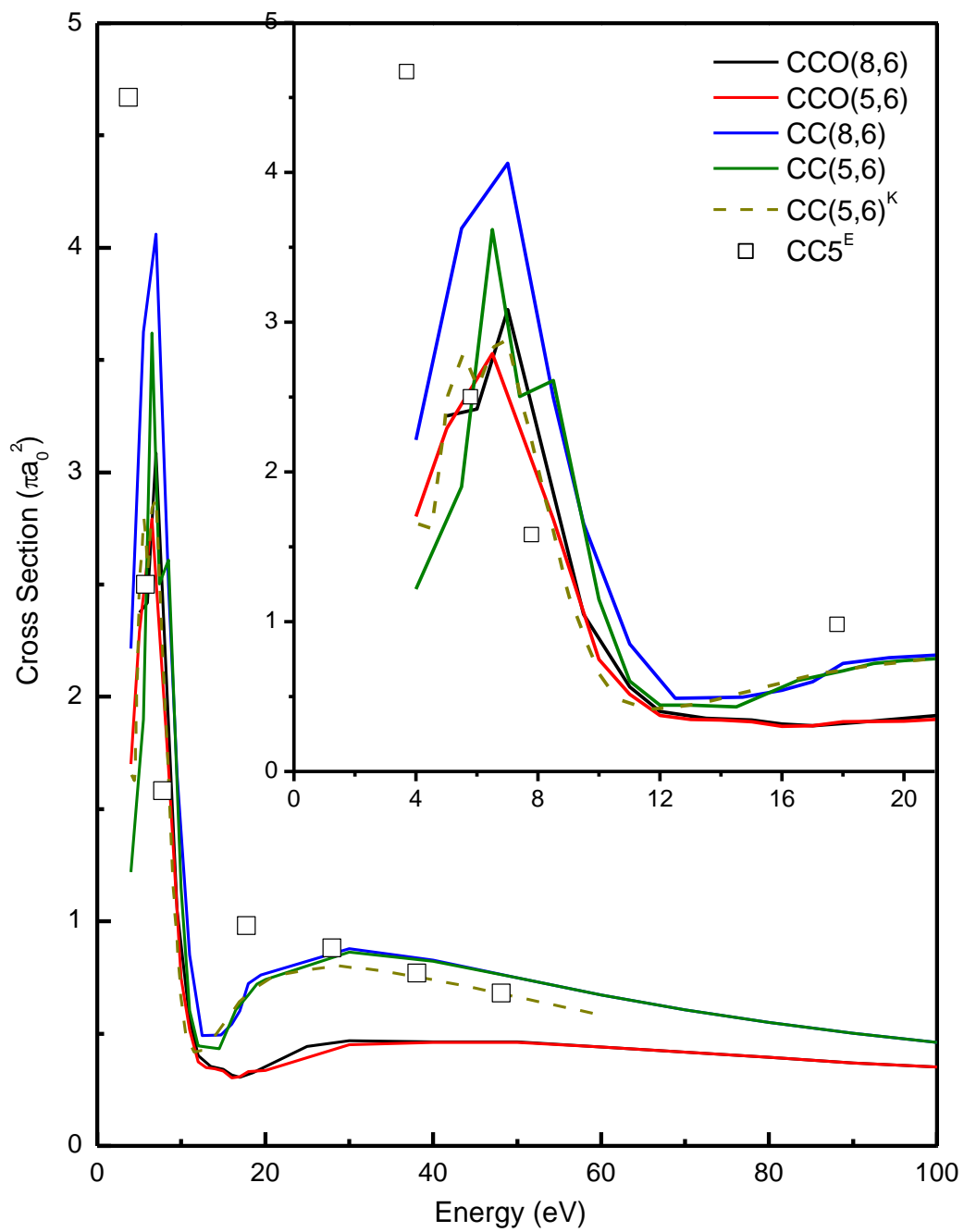


Fig. 5.14 : 5s – 6s excitation cross sections of positron-Rb scattering.

eV to 16 eV which can also be found in the cross section of the $CC(5,6)^K$ calculation. There are some notable quantitative discrepancies between the $CC(m,n)$ and $CC(5,6)^K$ calculations. The cross sections of the $CC(m,n)$ calculations are higher than the $CC(5,6)^K$ cross section at 4 eV to 12 eV (about 35% higher), as well as the energies higher than 20 eV (about 8% higher). The continuum effect is significant in this transition. The significance of the effect can be observed from some of the difference between the $CCO(m,n)$ and $CC(m,n)$ models from 10 eV onwards. Firstly, the predicted minimum of the $CCO(m,n)$ calculations is not as deep as the minimum of the $CC(m,n)$ and $CC(5,6)^K$ calculations. Secondly, the cross sections of the $CCO(m,n)$ calculations from 12 eV onwards are a lot lower than the $CC(m,n)$ calculations. At 30 eV, the $CCO(m,n)$ cross sections are almost 90% lower than the $CC(m,n)$ calculation, and the $CCO(m,n)$ and $CC(m,n)$ begin to converge as the energy increases. The difference between the $CCO(m,n)$ and $CC(m,n)$ calculations drops from 90% at 30 eV to 22% at 100 eV. Thus, we expect the cross sections of the $CCO(m,n)$ and $CC(m,n)$ models to converge at higher energies. The 6s transition accounts for a very minor portion of the TCS. In Table G.1 and G.2, we can see that its contribution to the TCS is less than 5.5% at the selected energies.

e) 6p Excitation Transition

Figure 5.15 displays the cross sections of 5s – 6p excitation. The $CCO(m,n)$ and $CC(m,n)$ calculations agree fairly well with the $CC(5,6)^K$ calculation. Our calculations show similar qualitative features as the $CC(5,6)^K$ calculation, where there is a minimum at 12 eV to 16 eV, followed by a maximum at around 25 eV. We note that the qualitative features of the cross sections of our present calculations at 10 eV and below do not agree well with each other. Similar phenomena can be seen in the K(5p) excitation (Ong (2006)) as well. Since this channel contributes relatively lesser to the

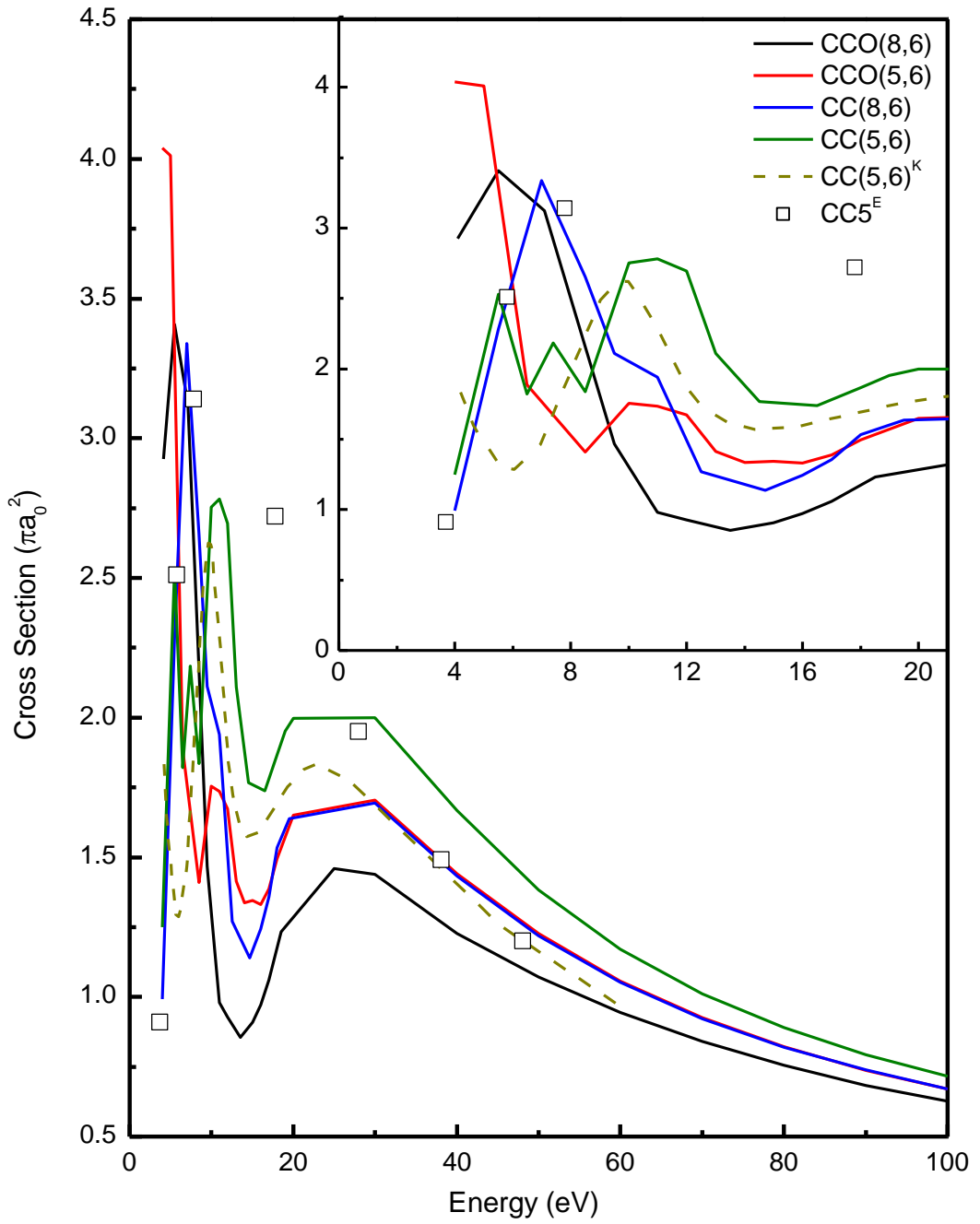


Fig. 5.15 : $5s - 6p$ excitation transition of positron-Rubidium scattering.

TCS compared to the other channels, it is unlikely that the inconsistency at the low energy region will be carried into the TCS. Similarly to the 6s transition, the 6p transition also contributes very little to the TCS (<2%) (refer to Table G.1 and G.2).

5.3.2 Positronium (Ps) Formation Cross Sections

The cross sections for the Ps formation in positron-Rb scattering are depicted in Figure 5.16 – 5.22. The cross sections of Ps(1s), Ps(2s), Ps(2p), Ps(n=3) and total Ps cross section will be discussed in detail. All the results will be compared to the available experimental and theoretical data.

a) Ps(1s) Formation

Figure 5.16 shows the cross section of Ps(1s) formation in positron-Rb scattering. We also show the DWA (post) and DWA (prior) (the distorted wave approximation) calculations in post and prior form, respectively (Guha and Mandal (1980)).

The present results are in good accord with the $CC(5,6)^K$ calculation but lower than the DWA calculation by 80% at 9 eV and 20 eV. In fact, the DWA cross sections are higher than all the other calculations. The CCO(m,n) models are converged with the CC(m,n) models, except in the energy region of 10 eV to 30 eV where the CCO(m,n) cross sections are lower than the CC(m,n) cross sections. We can observe that the Ps(1s) formation cross sections of all the data drops drastically from about $12\pi a_0^2$ at 4 eV to about $1.08\pi a_0^2$ at 10 eV and the cross section will become negligible as the energy increases. At 30 eV, the cross section is only about $0.18\pi a_0^2$ which is negligible. The Ps(1s) formation is even less significant with the inclusion of the continuum effect. The CCO(8,6) Ps(1s) formation cross section reaches as low as $0.23\pi a_0^2$ at 15 eV. So, the Ps(1s) formation is insignificant at energies lower than 30 eV and 15 eV for the

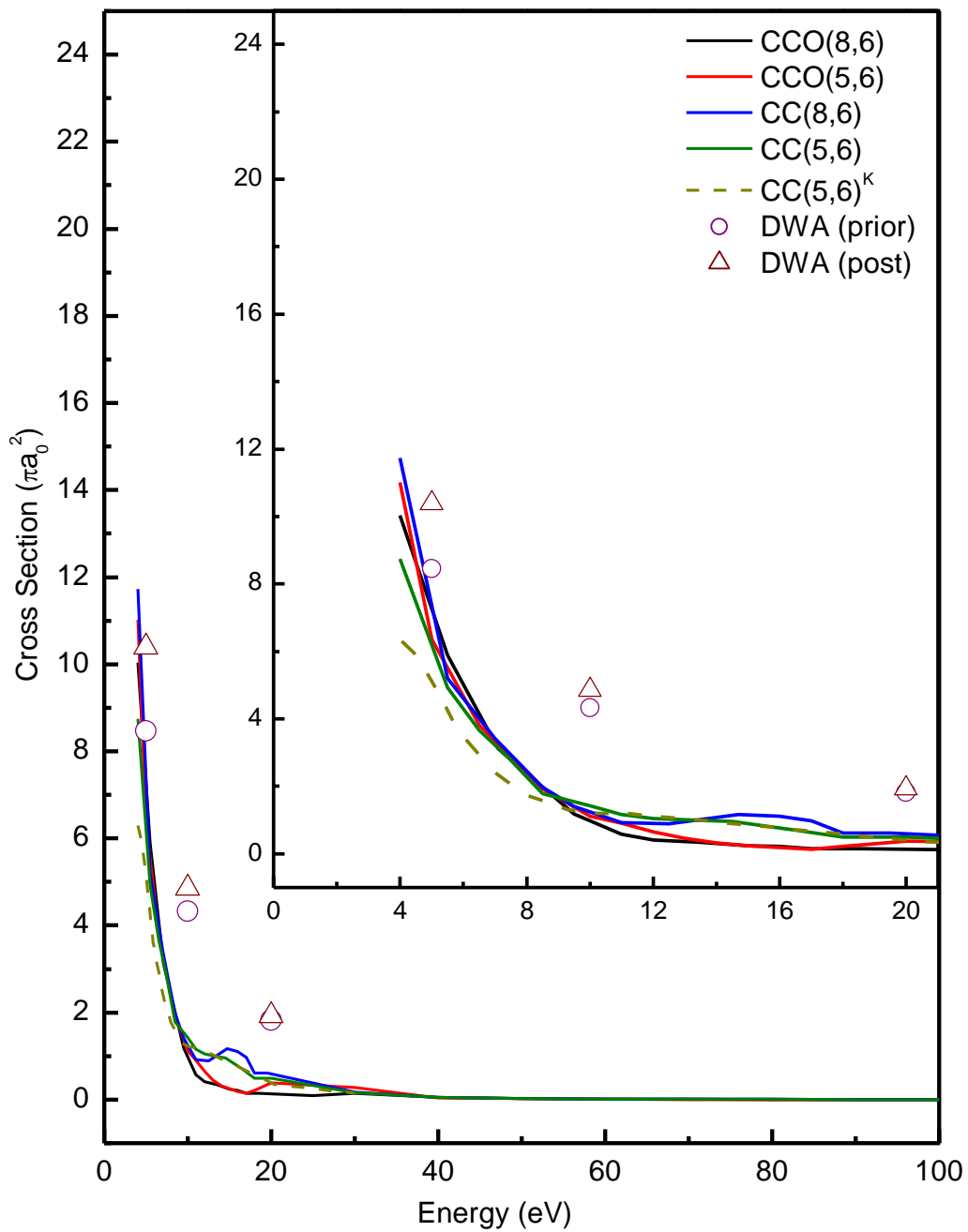


Fig. 5.16 : Ps(1s) formation of positron-Rb scattering.

CC(m,n) and CCO(m,n) calculations, respectively.

b) Ps(2s) Formation

Figure 5.17 shows the cross section of Ps(2s) formation for positron-Rb scattering. Generally, the present results are in qualitative agreement with the $CC(5,6)^K$ calculation where a predicted shoulder at 8 eV to 10 eV can be noted. Although our results predict a peak at 6 eV, it contrasts with that of the peak at 4 eV as seen in $CC(5,6)^K$. The CCO(5,6) model does not seem to be consistent with our other calculations. Although it has a shoulder, this is at 10 eV to 12 eV, and it is not obvious. Furthermore, the peak in this cross section is at 7 eV instead of 6 eV as in the other calculations. Obviously, both the CCO(m,n) and CC(m,n) cross sections are higher than the $CC(5,6)^K$ cross section, especially at the energy region of 5 eV to 10 eV. The CCO(m,n) calculations are lower in magnitude than the CC(m,n) calculations. This phenomena is reasonable as we had considered the continuum effect in the CCO(m,n) models. Similar to the Ps(1s) formation, the Ps(2s) formation is only significant at energies lower than 30 eV. From 30 eV onwards, the cross sections are negligible.

c) Ps(2p) Formation

The cross section of Ps(2p) formation is depicted in Figure 5.18. The present CCO(m,n) and CC(m,n) calculations are in fair agreement with the $CC(5,6)^K$ calculation. Overall, the present models' cross sections are higher than the $CC(5,6)^K$. There are some discrepancies at 4 eV to 10 eV but all the calculations converge at energies larger than 10 eV. We must note that all the calculations predict a peak but at different energy: CCO(8,6) and CC(8,6) at 5.5 eV, CCO(5,6) and CC(5,6) at 8.5 eV while $CC(5,6)^K$ at 7.5 eV. Similar to the Ps(1s) and Ps(2s) case, the cross section of Ps(2p) formation are relatively small when the energy goes beyond 30 eV and thus they are negligible at 30

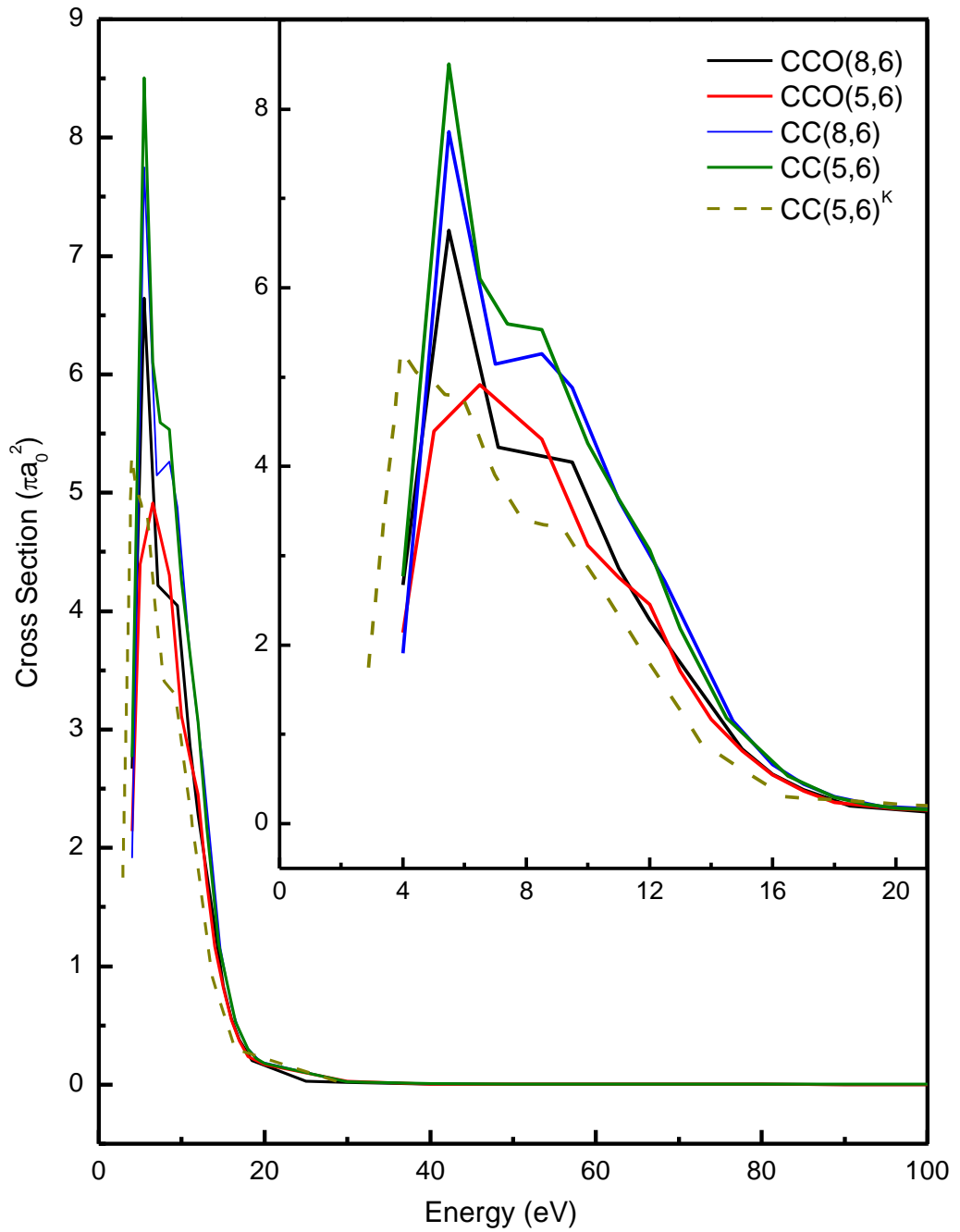


Fig. 5.17 : Ps(2s) formation of positron-Rb scattering.

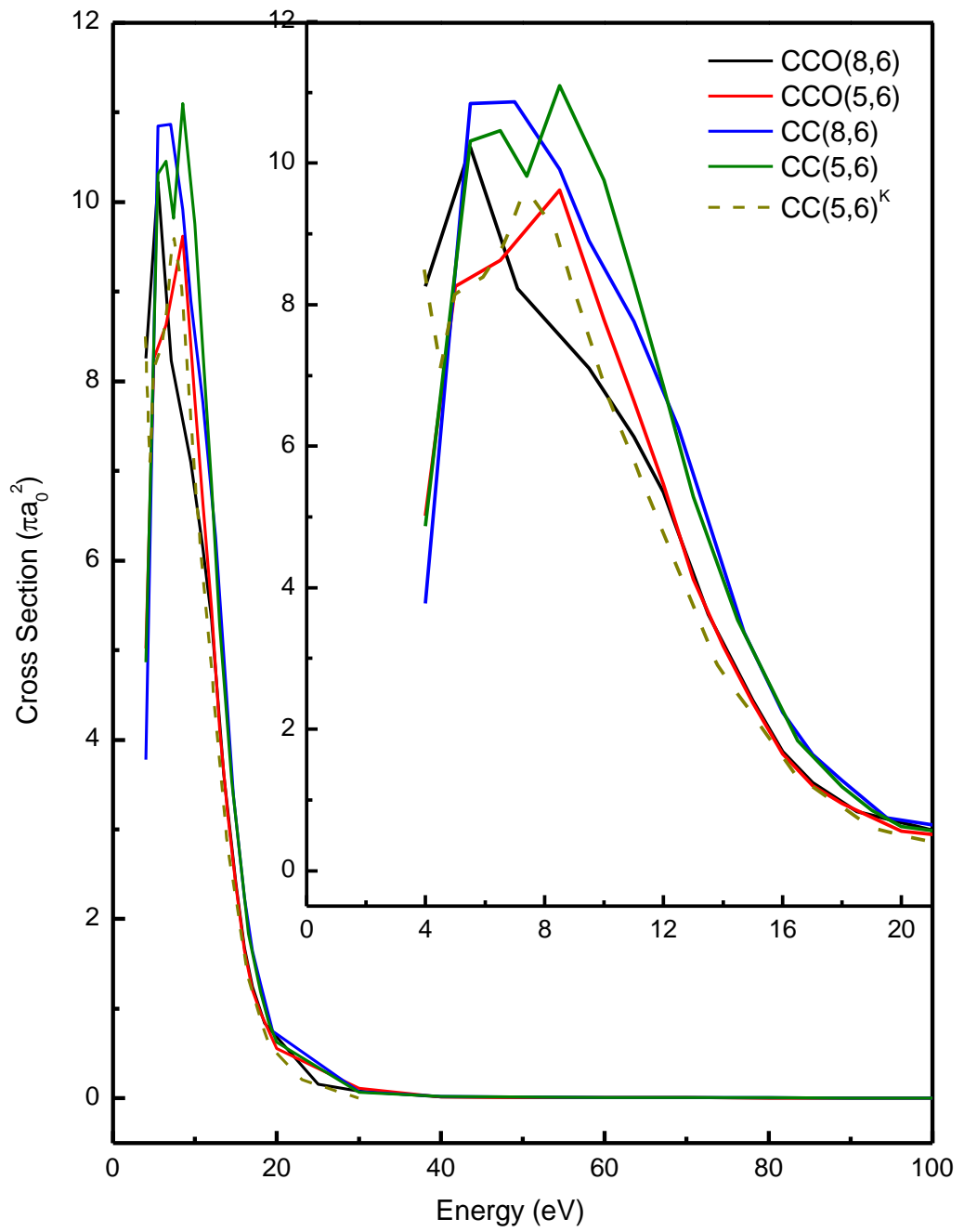


Fig. 5.18 : Ps(2p) formation of positron-Rb scattering.

eV onwards. The cross section of Ps(2p) formation have similar magnitude as in Ps(2s) formation, which means that this Ps formation is as important as Ps(2s) formation in the positron-Rb scattering. From Table G.1 and G.2, we note that the Ps(n=2) formation is the dominant transition among the Ps formation at energies lower than 10 eV.

d) Ps(n=3) Formation

The cross section of Ps(n=3) formation is depicted in Figure 5.19. In general, the present calculations have decent agreement with the CC(5,6)^K calculation. All the calculations display a peak in the low energy region. But, the energy at which the peak is formed is different for all the calculations. The magnitudes of the peak are various as well. The continuum effect brings down the cross section at energies larger than 10 eV which makes the discrepancies between the CCO(m,n) and the CC(5,6)^K calculation smaller. Once again, the Ps(n=3) formation is insignificant at energies larger than 30 eV.

e) Total Positronium Cross Sections (TPCS)

Figure 5.20 shows the TPCS for positron-Rb scattering. The CC(5,6)^{K1} is the R-matrix calculation for Ps(n=1)+Ps(n=2)+Ps(n=3) formation cross section (Kernoghan *et al* (1996)). The LL and UL-R are the experimental measurements done by Surdotovich *et al* (1996) which represent the Lower Limit and improved Upper Limit, respectively. The present results agree well with the CC(5,6)^{K1} calculation as the present calculated Ps(n=1), Ps(n=2) and Ps(n=3) formations cross sections also agree well with the CC(5,6)^K. It is encouraging to observe that the continuum effect lowers the TPCS of the CCO(m,n) calculations by 25% compared to the CC(m,n) calculations. This effect causes the CCO(m,n) calculations to agree better with the experimental and theoretical data, especially at 8 eV to 16 eV. The present calculations demonstrate a peak at the energy region of 5 eV to 8 eV, which is also reflected in the CC(5,6)^{K1} calculations. Thus, it will be reasonable to find a peak in this energy region in the TPCS

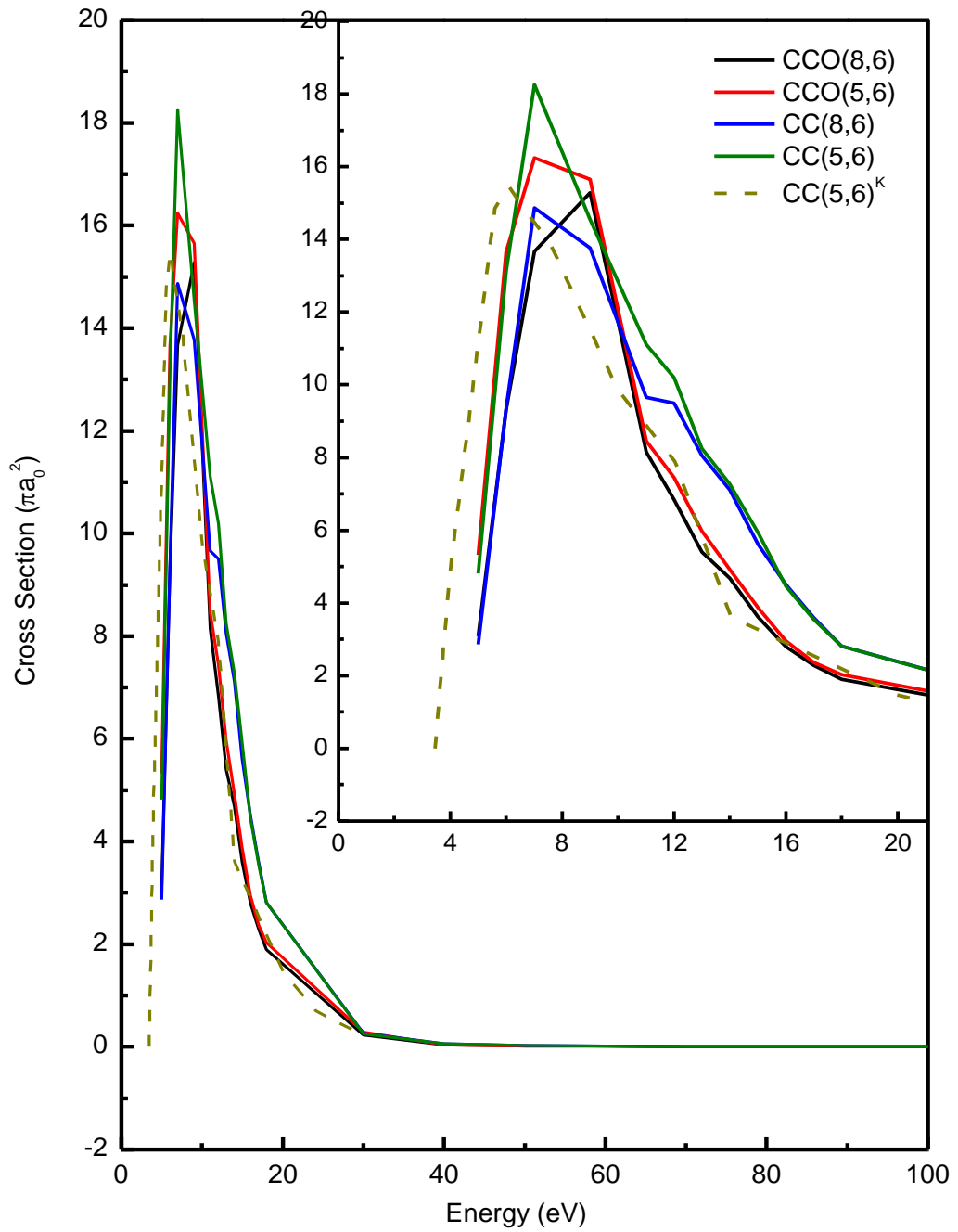


Fig. 5.19 : Ps(n=3) formation of positron-Rb scattering.

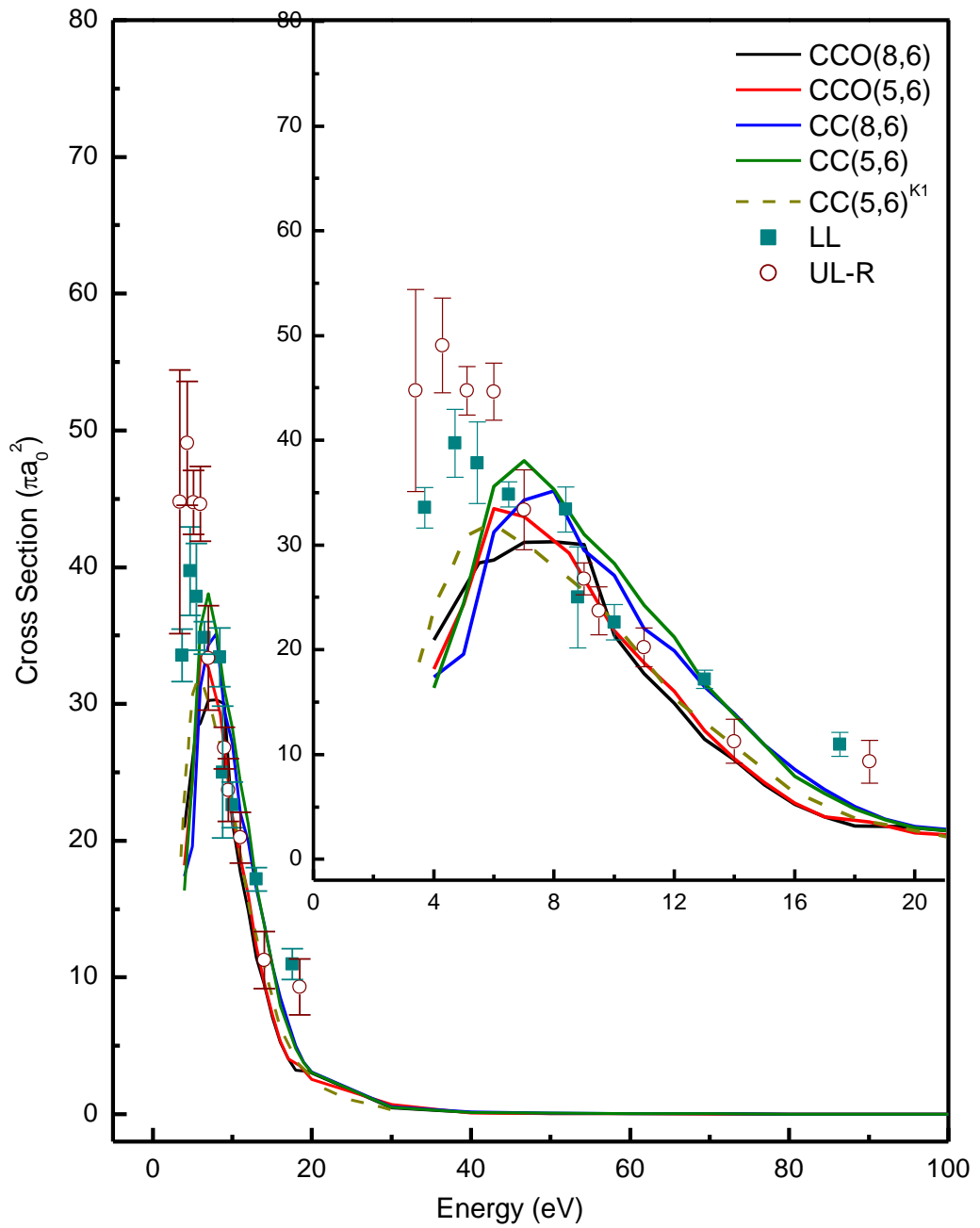


Fig. 5.20 : Total Ps cross section of positron-Rb scattering.

as well. Although the present calculations successfully predict a peak for the TPCS, but this peak is formed at a larger energy region compared to the LL and UL-R measurements (which shows the peak to be at around 4.5 eV). At energies lower than 6 eV, the present calculations underestimate the TPCS. Our results are about 40% lower than the LL measurement at that energy region. It is not surprising to find that the TPCS drop drastically as the energy increases because the same phenomena can be found in all the Ps formations. The TPCS is negligible at energies higher than 30 eV.

It can be noted from Table G.1 that the TPCS accounts for a maximum of 15.45% of the TCS. The contribution of the TPCS to the TCS in the CCO(8,6) calculation shown in Table G.1 is slightly lower (12.39%) than the CC(8,6) calculation. This is interesting as in the noble gas cases, the cross sections of the Ps channels can contribute more than 40% to the TCS (Kauppila *et al.* 1981, Dababneh *et al.* 1982, Marler *et al.* 2005). This is due to the continuum effect as it allows the flux to be absorbed into more open channels.

5.3.3 Total Cross Section (TCS)

Figure 5.21 shows the TCS of the positron-Rb scattering. MG3 is the modified Glauber approximation in the frozen core approach by Gien (1993). CCO^Z is the coupled-channel optical calculation done by Zhang *et al.* (2007). Parikh *et al.* (1993) is the experimental group that measured the TCS of the positron-Rb scattering.

Generally, the CCO(m,n) and CC(m,n) are in good agreement with the other theoretical data, except the PFMP and MG3 models which are 35% and 20% lower than the present calculations, respectively. The other theoretical results are within 10% when compared to our results. The present calculations do not agree well with the experimental measurement quantitatively, where it overestimates the TCS by 38% at the 4 eV to 20 eV energy region. At 20 eV to 100 eV, the CC(m,n) calculations converge

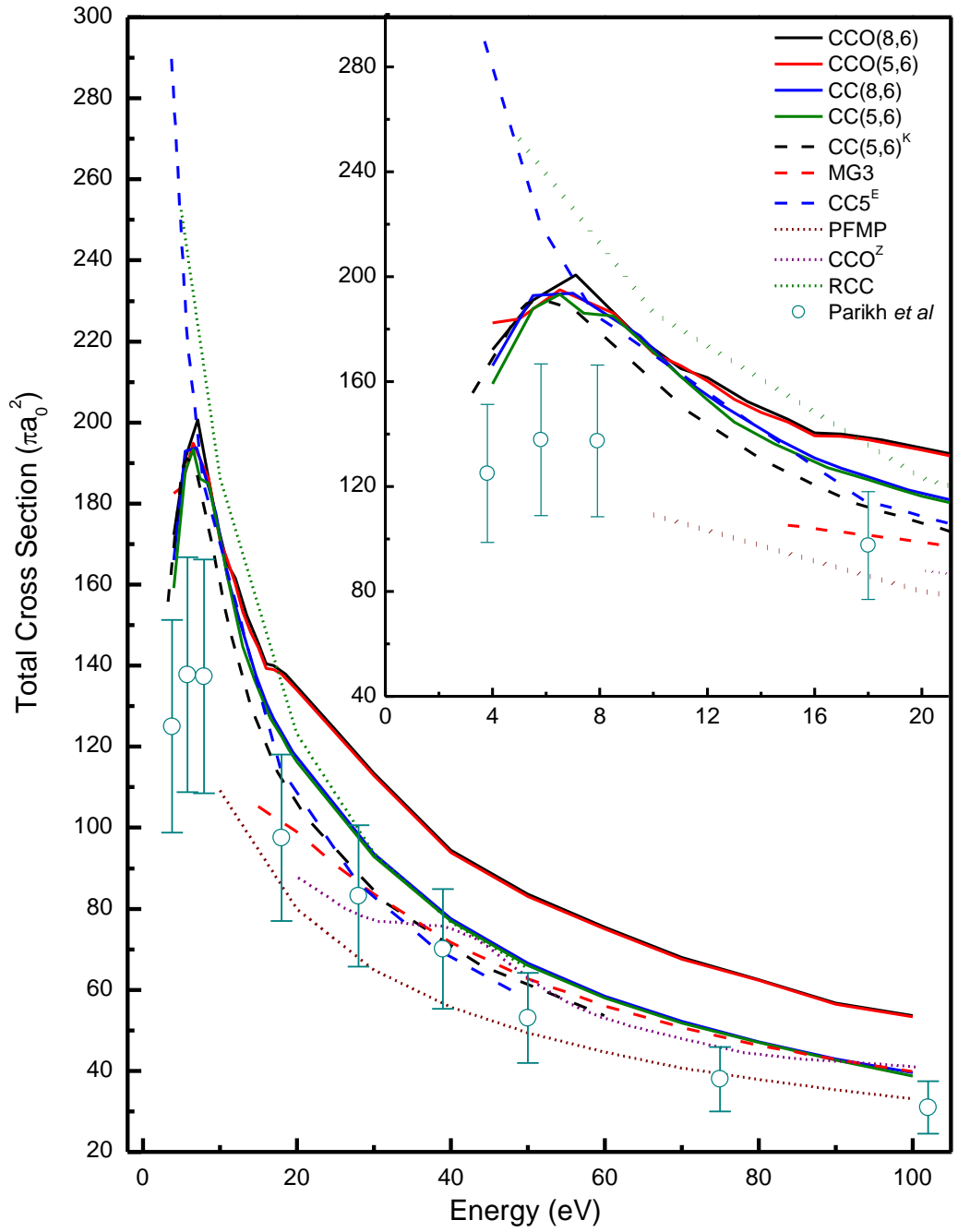


Fig. 5.21 : Total cross section of positron-Rb scattering.

with the MG3, CCO^Z and RCC calculations. The $CC(m,n)$ calculations remain 9% higher than $CC(5,6)^K$ and $CC5^E$ throughout the energy region. Although the discrepancies between the $CC(m,n)$ TCS and the experimental measurement decreases as the energy increases, but it is still about 25% higher than the experiment data at 75 eV. The reason of the discrepancies is due to the fact that Parikh *et al.* (1993) do not include the angular-discrimination considerations into their measurement. The effects of the forward angle scattering on the TCS are discussed in Section 5.2.2. So, the measured TCS of Parikh *et al.* (1993) could be considered as a lower limit to the TCS. We are certain that the difference between the present calculations with the experimental data will be decreased when the angular-discrimination is taken into account in the experiment. The $CCO(m,n)$ calculations which includes the continuum effect into the calculations have higher TCS compared to the other results especially at energies higher than 20 eV. The continuum effect has increased the TCS as we have taken into account the lost flux which is absorbed into the continuum channels. The $CCO(m,n)$ calculations are about 22% higher than the $CC(m,n)$ calculations at 20 eV and above. The discrepancies remain throughout the whole energy region. This indicates that the continuum effect is significant even at high energies.

We observe a peak at around 6 eV in the $CC(m,n)$, $CCO(m,n)$ and $CC(5,6)^K$ TCS, which is also shown in the experimental data as well. The existence of this peak can be explained by the similar peak displayed in the TPCS (Figure 5.22). We believe that the peak in the TCS is substantially caused by the $Ps(n=2)$ and $Ps(n=3)$ formations. The $5s - 4d$ and $5s - 6s$ excitations also contribute to the formation of this peak in the TCS.

5.3.4 Differential Cross Section (DCS)

a) Ps(1s) Formation

Figure 5.22 and 5.23 show the DCS of Ps(1s) formation for positron-Rb scattering at 5 eV and 10 eV. DWA (prior) and DWA (post) are the distorted-wave approximation calculations in the prior and post form, respectively (Guha and Mandal (1980)).

The present calculations do not agree very well with the DWA calculations at both energies. At 5 eV, our results show good agreement with the DWA (post) calculation at the forward scattering angles ($0^{\circ} - 15^{\circ}$). Both CCO(8,6) and CC(8,6) models predict a minimum at around 25° which is also shown in the DWA (post) calculation. At angles larger than 35° , there are major discrepancies between the present calculations and the DWA calculations, where our DCS display serious fluctuations. The CCO(8,6) calculation have slightly higher DCS at the forward scattering angles than the CC(8,6) calculation. The minimum of CCO(8,6) model at $\sim 25^{\circ}$ is also a lot deeper. Due to the fluctuations in the DCS, it is hard to analyse the continuum effect in the DCS at 5eV.

At 10 eV, our results agree well with the DWA (post) calculation at the forward scattering angles. It is encouraging to see that the present calculations can once again predict the minimum at the forward angles. The fluctuations at the larger angles are not so serious compared to the fluctuations at 5 eV. The continuum effect increases the DCS at the forward angles ($0^{\circ} - 15^{\circ}$), but the CCO(8,6) calculation has overall lower DCS than the CC(8,6) calculation.

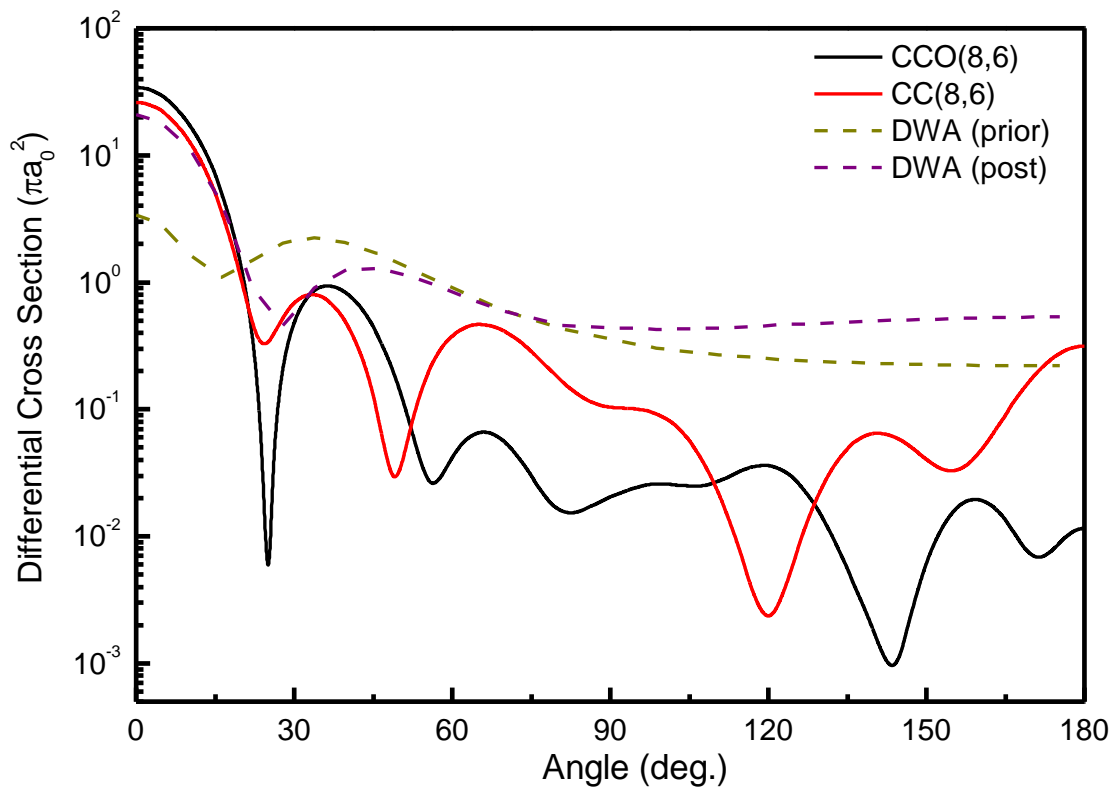


Fig. 5.22 : DCS of Ps(1s) formation for positron-Rb scattering at 5 eV.

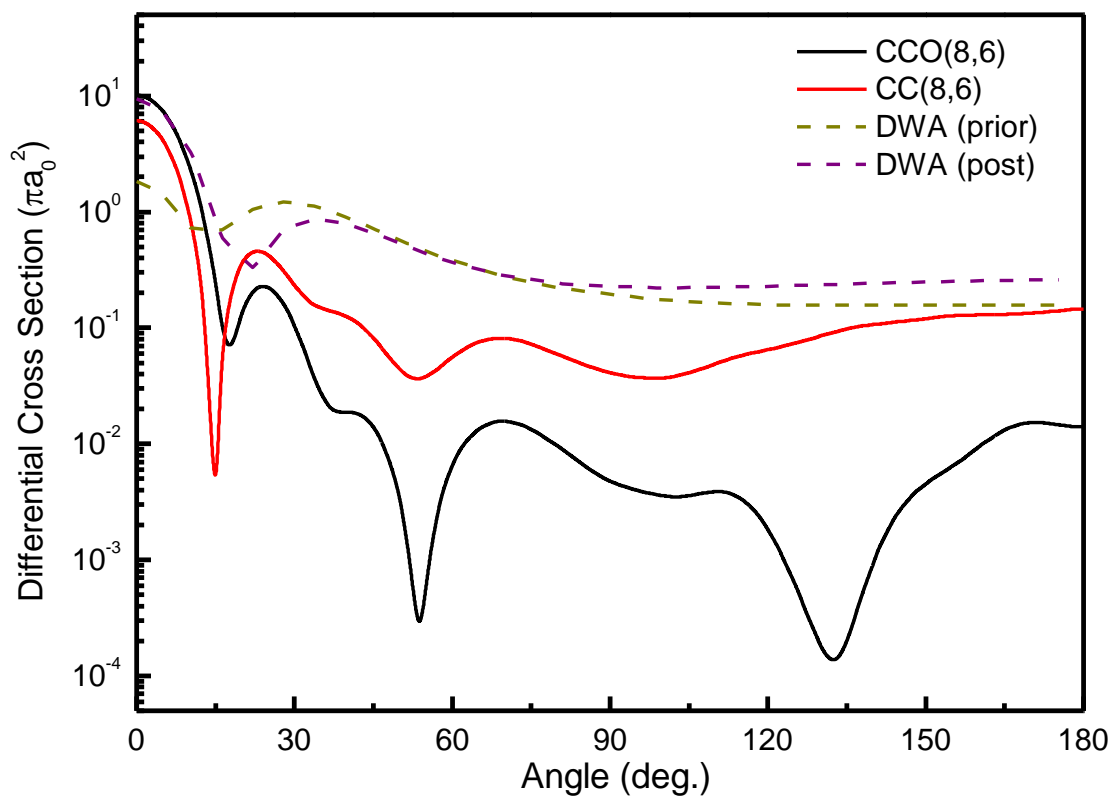


Fig. 5.23 : DCS of Ps(1s) formation for positron-Rb scattering at 10 eV.

b) 5s Elastic Transition

Figure 5.24 and 5.25 show the DCS for elastic scattering of positron-Rb scattering at 5 eV, 10 eV and 20 eV. Generally, the CCO(8,6) and CC(8,6) calculations exhibit similar qualitative features. However, there are some discrepancies between these models. At 5 eV, the minimum displayed by the CCO(8,6) calculation at the middle scattering angle is far deeper than the minimum shown by CC(8,6). At 10 eV, the CCO(8,6) calculation predict 2 minima at the middle angles. In contrast, the CC(8,6) calculation does not predict any minimum at those scattering angles. It can be noted that the same phenomena can be observed in the scattering region of $20^\circ - 80^\circ$ at 20 eV. The continuum effect in the CCO(8,6) model does not only alter the features of DCS, it also lowers the overall magnitude of the DCS. As we do not have any theoretical and experimental data to compare with the present calculations, thus we cannot verify the qualitative features and the magnitude of the DCS.

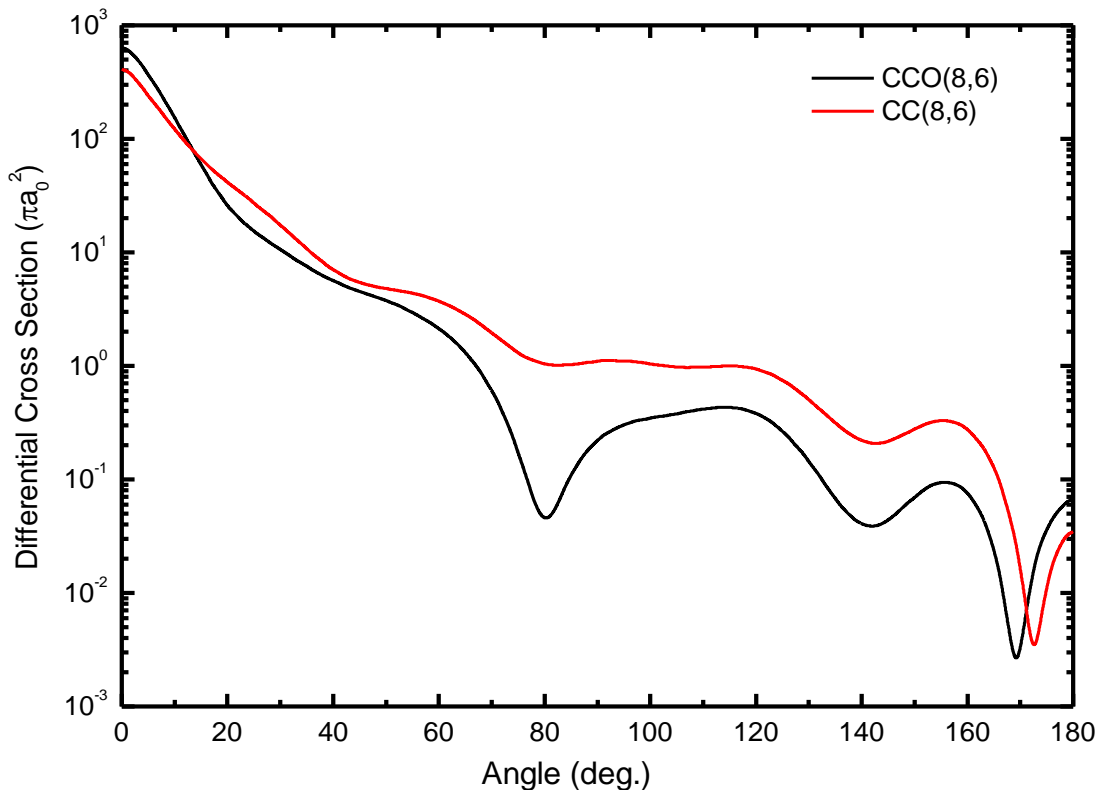


Fig. 5.24 : DCS of elastic scattering for positron-Rb scattering at 5 eV.

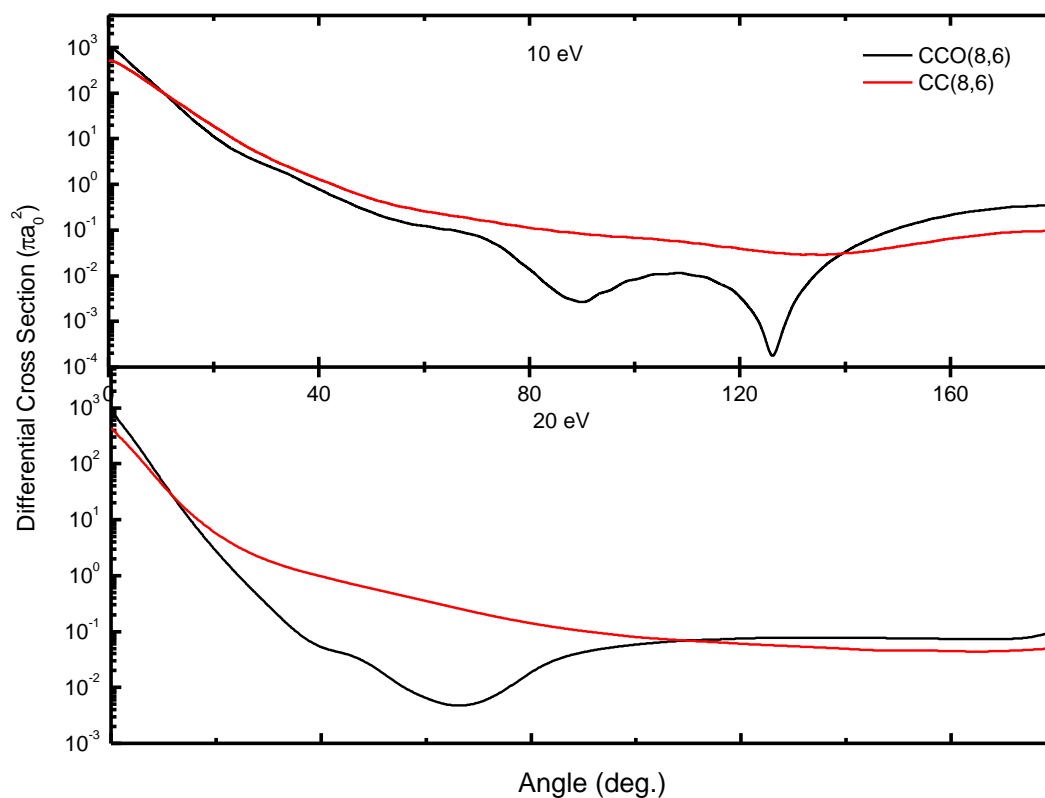


Fig. 5.25 : DCS of elastic scattering for positron-Rb scattering at 10 eV and 20 eV.

c) 5p Excitation Transition

The DCS of 5p excitation for positron-Rb scattering at 10eV and 20 eV are depicted in Figure 5.26 and 5.27. DWM is the distorted-wave method implemented by Pangantiwar *et al.* (1988).

At 10 eV, the present models agree qualitatively with the DWM model. Quantitatively, both models' DCS are smaller than the DWM calculation over the whole scattering angles. At 20 eV, the present calculations show good agreement with DWM calculation. At both of the incident energies, the continuum effect brings down the overall DCS. Thus, it can be noted that the CCO(8,6) calculations are generally lower than the other calculations.

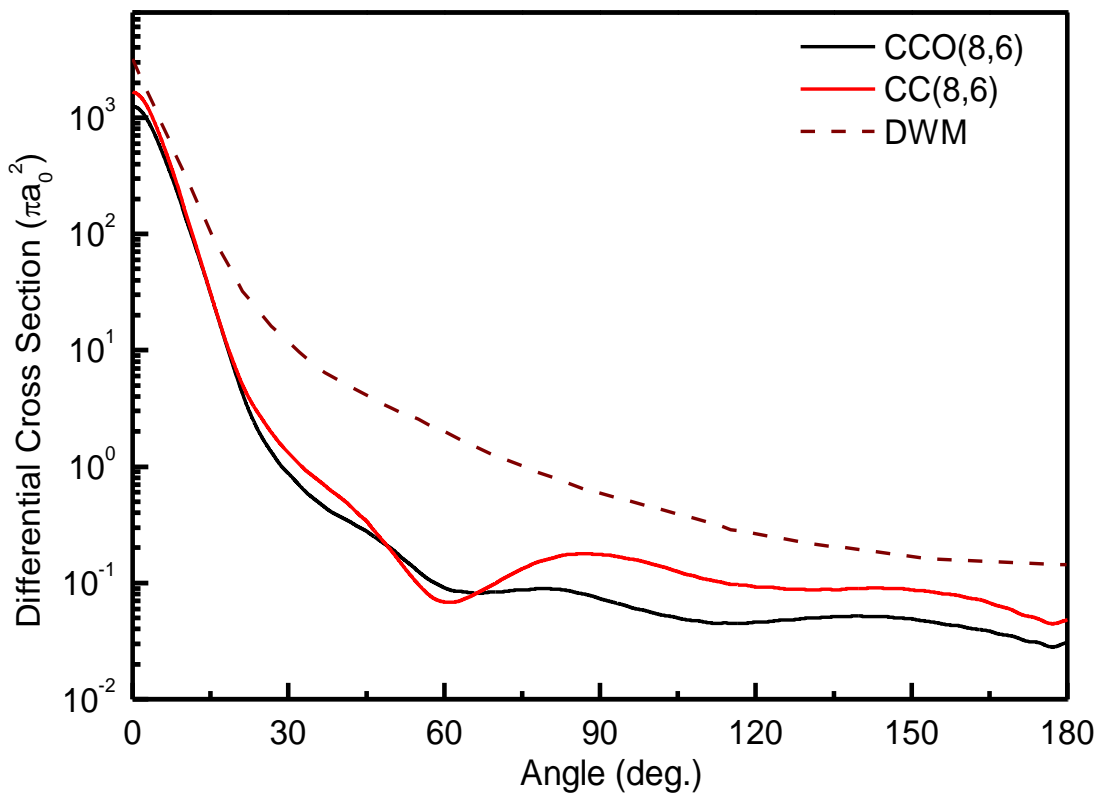


Fig. 5.26 : DCS of 5p excitation for positron-Rb scattering at 10 eV.

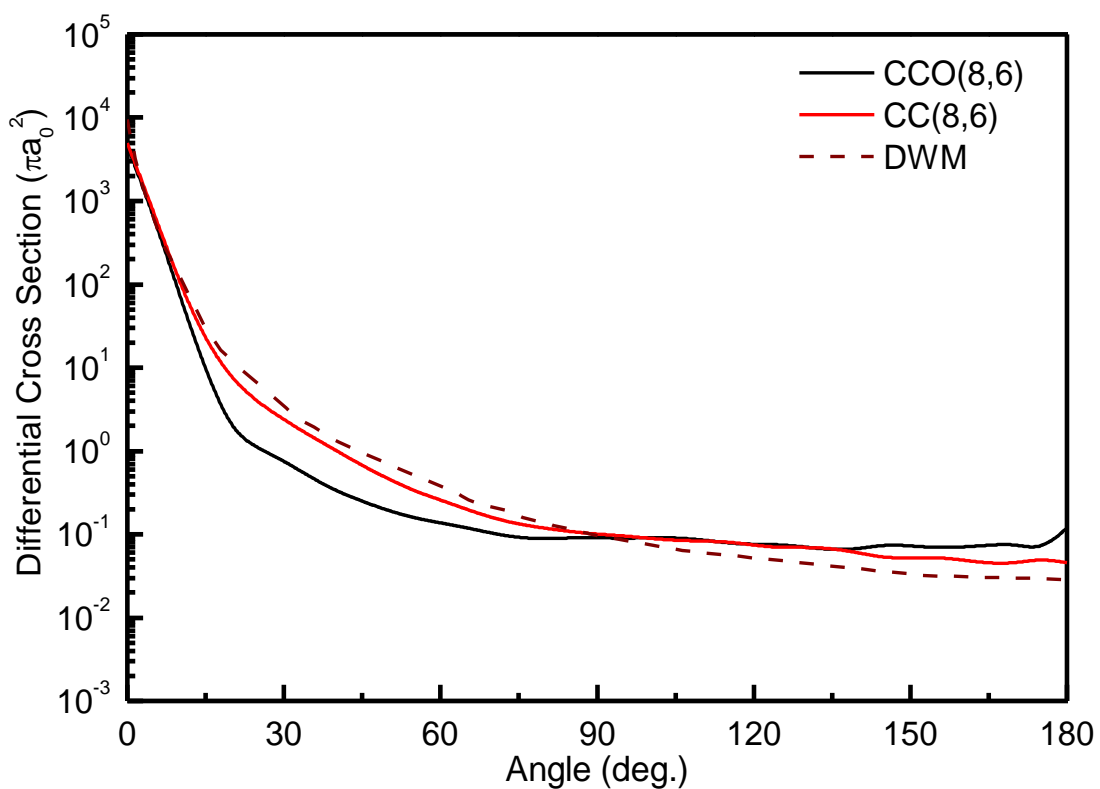


Fig. 5.27 : DCS of 5p excitation for positron-Rb scattering at 20 eV.

CHAPTER 6

Conclusion

In this thesis, the coupled-channel optical method (CCOM) has been used in the study of electron or positron scattering from rubidium atom (Rb). Various calculations have been done to investigate different physical observables. For electron-Rb scattering, the CCO5 and CCO8 calculations which implement the CCOM method are carried out at 4 – 100 eV. For positron-Rb scattering, the CCO(5,3), CCO(5,6), CCO(8,3) and CCO(8,6) calculations have been used in the energy range of 4 – 100 eV.

For electron-Rb scattering, we have calculated the elastic, inelastic, differential and total cross sections. In general, the present calculations are in good agreement with the available experimental and theoretical data. We do not have any available data to compare with the present calculations for the elastic and inelastic cross sections. But, we can observe that the continuum effect is important as reflected in the variation of the magnitude of the cross sections in all the transitions. It can also be noted that the 5p channel is the dominant channel in the electron-Rb scattering system at all the energies except at 4 eV. It is encouraging to note that the TCS of the CCO8 calculation is higher in magnitude than the other calculations and it agrees better with the experimental data (if the angular-discrimination is considered in the experiments). Nonetheless, more experimental as well as theoretical data are needed.

For positron-Rb scattering, we have investigated in depth the cross sections for most of the channels. The DCS, TPCS and TCS of the calculations have been presented as well. In contrast with the electron case, there are more positron-Rb experimental and theoretical data available to compare with the present calculations. The calculation of Kernoghan *et al.* (1996) can be considered as the gauge for the validity of the present calculations as the R-matrix calculations reported extensive data for most transitions.

The present calculations agree qualitatively well with those of Kernoghan *et al.* (1996) but there are some discrepancies in the quantitative aspects. The discrepancies are plausibly due to the continuum effect. Another possibility is the omission of the core-exchange effect. An investigation on this effect might be carried out in the future.

The present calculations are in good accord with the work of Kernoghan *et al.* (1996) as it also shows that the Ps(n=1) formation is not the major contributor for the Ps formation in the positron-Rb scattering system. Most of the Ps formation cross sections are from the Ps(n=2) and Ps(n=3). The present results also support the existence of a peak at 6 eV in the TCS which is mainly due to the Ps formation.

Generally, the inclusion of higher atomic states (Rb(5d), Rb(7s), Rb(7p)) in the calculations does not affect the overall results of the calculations very much, both quantitatively and qualitatively. However, as expected there are significant changes in the cross sections of some channels at 5 – 20 eV with the inclusion of these higher states. So, these higher states cannot be ignored. The CCO(8,6) calculation is by far the largest calculation that has been reported for the investigation of positron-Rb scattering.

The continuum effect is very important in the positron-Rb scattering. This effect is observable in every single channel of the scattering system. The continuum effect is most prominent in the TCS where the CCO(8,6) TCS is significantly larger than the other calculations. It is undeniable that the continuum effect is essential in the realistic approach of the scattering problems but there is no experimental data to verify the improvement in the TCS made by this effect. The experimental measurement done by Parikh *et al.* (1993) does not include the angular-discrimination considerations into the measurement, thus their TCS would always be lower than the exact TCS. So, experimental measurements which allow for the angular-discrimination considerations are highly desirable.

The DCS results were reported for selected transitions and energies as there are only limited available theoretical and experimental data. The present calculations' DCS does not agree very well with the other theoretical calculations. Nevertheless, it is encouraging to see that the CCO(8,6) DCS agrees fairly well with the DWM DCS in the 5p excitation transition at 20 eV.

In conclusion, we have achieved our objectives in successfully implementing the CCOM in the study of positron-Rb scattering by showing satisfactory results in the calculations. However, we caution that Rb is a large atomic system and a relativistic approach may be used in future work.

Appendix I

